1966

A periodic type of microwave sampling cavity

Allan George Potter
Iowa State University

66–6995

POTTER, Allan George, 1930–

A PERIODIC TYPE OF MICROWAVE SAMPLING CAVITY.

Iowa State University of Science and Technology
Ph.D., 1966
Engineering, electrical

University Microfilms, Inc., Ann Arbor, Michigan

A PERIODIC TYPE OF MICROWAVE SAMPLING CAVITY

by

Allan George Potter

A Dissertation Submitted to the
Graduate Faculty in Partial Fulfillment of
The Requirements for the Degree of
DOCTOR OF PHILOSOPHY

Major Subject: Electrical Engineering

Approved:

Signature was redacted for privacy.

In Charge of Major Work

Signature was redacted for privacy.

Head of Major Department

Signature was redacted for privacy.

Dean of Graduate College

Iowa State University
Of Science and Technology
Ames, Iowa

1966

TABLE OF CONTENTS

INTRODUCTION

During the last fifteen years various properties of gaseous media have been measured using microwave cavities as the sampling device. Although extensive work has been done in this field with respect to the design of refractometers and microwave spectrometers, very little effort has been directed toward the determination of the variation of sampling cavity characteristics caused by opening it to the sampled medium. In this paper, a special type of spaced-ring cavity will be analyzed and the limits to which it may be opened to the sampled medium examined in detail.

This particular type of microwave cavity was considered because it offers the possibility of increasing the ratio of open to closed cavity surface and at the same time reducing the temperature dependence of its resonant frequency. The fact that more open surface may be possible without seriously degrading the desirable characteristics of a cavity is most attractive when one considers the turbulence problem present when measuring the properties of gaseous media under flow-through conditions. For this type of measurement, minimum turbulence along with rapid response are usually desired so that cyclic changes may be accurately recorded. One of the most promising uses being considered for this type of cavity is the measurement of the partial pressure of the various polar gases in expired air.

A spaced-ring type of waveguide structure made up of

insulated concentric rings was first studied by Fox, Miller, and King of the Bell Telephone Laboratories while working on a problem in wideband communications via cylindrical waveguide at microwave frequencies. Since low attenuation was the paramount factor in their study, they chose a cylindrical waveguide operating in the TE_{01} mode because this mode has the property of decreasing attenuation with increasing frequency above cutoff. The attenuation for this mode is given by

$$(1) \qquad \alpha_{TE_{01}} = \frac{R_s \, (f_c/f)}{a\eta\sqrt{1-(f_c/f)^2}}$$

where R_s = surface resistance (ohms),

η = intrinsic impedance of medium inside the waveguide (ohms),

f_c = cutoff frequency for TE_{01} waveguide mode (cps),

f = operating frequency (cps),

and a = radius of waveguide (meters).

It was shown in their studies that a 2db per mile loss at a frequency of 50 KMC for a 2 inch diameter brass pipe using the TE_{01} mode is possible. However, it was also found that mode switching was present if any imperfections existed in the guide wall. Such mode switching causes both phase distortion and unwanted power losses of the desired mode. This problem is particularly acute in elements used to traverse corners. To reduce signal losses and interference effects due to mode conversion and reconversion, dissipation was introduced to the

unused modes on a continuous basis. Several ways of doing this were found. One of these is a spaced-ring type of circular waveguide made of concentric isolated metal rings which provide a boundary which is preferential to the TE_{on} family of modes. All modes other than the TE_{on} circular type have wall currents in the longitudinal direction and experience considerable loss in the spaced-ring structure as compared to the loss in a solid-walled guide. The power loss for the spaced-ring structure under proper conditions was observed to be about 60 per cent more than the theoretical loss for an ideal copper tube, whereas the observed loss for the unused modes of propagation was on the order of 1000 to 5,000 times the TE_{01} value. The higher-order circular waves (i.e. TE_{02}, TE_{03} ....) exist with losses comparable to their values in a solid pipe, but fortunately the magnitudes of conversion between the TE_{01} and other TE_{on} modes have been found to be quite small.

Because of these facts, it seemed reasonable to assume that a spaced-ring structure could be used to advantage as an open sampling cavity. If the insulated rings can be made progressively thinner without impairing the desirable characteristics of the cavity, then it should be possible to achieve low turbulence to gas flow and better resonant frequency stability with this type of unit. A TE_{01p} mode in this type of structure is also optimum with regard to the detrimental effects caused by the adsorbed water vapor and absorbed gas at the guide wall. This is true because the $\vec{E}$ field for this

type of mode is zero at the guide wall and the cavity wall surface area is minimized in this application, respectively.

In the sections to follow, the important uses and characteristics of this type of cavity will be examined. In particular the applications of sampling cavities, measurement techniques, and systems using sampling cavities will be presented in order to provide a basis for the interpretation of the results of the analysis to follow. In this analysis the field approach will be utilized to develop a so-called condition equation. The solution of this equation will then allow us to express in an approximate fashion the fields inside and outside the cavity in terms of space harmonics. We can then, in a straight forward manner, derive equations for cavity quality factor (Q_o) and resonant frequency (f_r). Using these equations one can then determine the effects of various cavity parameters on the desirable characteristics of this particular type of sampling cavity.

SAMPLING CAVITY APPLICATIONS

There are several fields of study where quantities of interest may be obtained by using a microwave sampling cavity as a measurement device. Among those of interest to the field of radio propagation in the microwave region are the refractive index and the absorption characteristics of the transmission medium.

Refractive Index

The refractive index of a medium is related to the relative dielectric constant by the following equation

$$(2) \qquad n = \sqrt{\epsilon_r}$$

where n = refractive index

and ϵ_r = relative dielectric constant.

Another quantity which is sometimes used instead of the refractive index is called the refractivity and is defined by the equation

$$(3) \qquad N = (n-1)\ 10^6.$$

This quantity is used because the value of n for nearly all gaseous media only differs from unity by a very small amount.

The measurement of refractive index using a sampling cavity depends upon the fact that the resonant frequency of a cavity is related to the relative dielectric constant of the medium inside the cavity by the relationship

$$(4) \qquad f_r = \frac{\alpha}{\sqrt{\epsilon_r}} = \frac{\alpha}{n}$$

where α = a constant

and f_r = resonant frequency (cps).

If we take the derivative of Equation 4 with respect to n one can show that

$$(5) \qquad \Delta f_r \cong \frac{-\alpha \Delta n}{n^2} \cong -(\alpha 10^{-6})\Delta N,$$

since $n^2 \cong 1$ for most gaseous media.

This last equation expresses the fact that the change in resonant frequency is directly proportional to the change in refractivity. If one measures Δf with respect to the resonant frequency for the case where the cavity medium is a vacuum then $N = \Delta N$ and one can obtain N directly from the measurement of the shift in resonant frequency.

One of the many possible applications of the refractivity measurement in a gaseous media involves the determination of the partial pressure of water vapor contained therein. This can be accomplished by using the empirically determined equation

$$(6) \qquad N = \frac{77.6}{T}\left[P + \frac{4810}{T} P_{H_2O}\right]$$

where N = refractivity,

T = absolute temperature (K^o),

P = total pressure (millbars),

and P_{H_2O} = partial pressure of water vapor (millibars).

From Equation 6 it is apparent that if the total pressure and temperature are held constant then

$$(7) \qquad N = \alpha_1 + \alpha_2 P_{H_2O}$$

where α_1 and α_2 are constants. Thus a microwave hygrometer can be realized in this manner by measuring Δf. If we wish to measure P_{H_2O} in an absolute manner then Δf must, of course, be zero when P_{H_2O} is zero. An instrument of this type has been developed by Magee and Crain (10) and reported in the Review of Scientific Instruments.

Microwave Absorption

It is well known that the molecules of most gases possess absorption spectra in the microwave region. The bandwidth and amplitude of these spectral lines are affected by several factors such as natural line breadth, doppler effect, pressure broadening, and wall collisions. By far the most important of these is the pressure broadening effect which can be quantitatively expressed by the equation

$$(8) \qquad \gamma = \frac{8\pi^2 Nm}{3ckT} \left|\mu_{ij}\right|^2 f^2 \left[\frac{\frac{1}{2\pi\tau}}{(f-f_r)^2 + \left(\frac{1}{2\pi\tau}\right)^2} + \frac{\frac{1}{2\pi\tau}}{(f+f_r)^2 + \left(\frac{1}{2\pi\tau}\right)^2} \right]$$

where γ = absorption coefficient (neper/cm),

N = number of molecules per cm^3,

m = fraction of molecules in excited state,

c = velocity of light (cm/sec),

k = Boltzmann constant (joules/^{o}K),

T = absolute temperature (^{o}K),

$|\mu_{ij}|^2$ = square of dipole moment matrix element summed over directions

f = frequency (cps),

f_r = resonant frequency (cps),

and τ = mean life time between collisions (sec).

In the region near to f_r with $\Delta f \ll f_r$ Equation 8 can be approximated by

$$(9) \qquad \gamma \cong \frac{8\pi Nm}{3ckT} |\mu_{ij}|^2 f^2 \left[\frac{\Delta f}{(f-f_r)^2 + (\Delta f)^2}\right].$$

This is the form of a typical resonance absorption of half bandwidth $\Delta f = \frac{1}{2\pi\tau}$. It can be seen from this equation that the absorption peak (γ_{max}) at the resonant frequency (f_r) is proportional to N and inversely proportional to $1/2\pi\tau$. Now at low pressures both N and $\frac{1}{2\pi\tau}$ are proportional to pressure, therefore, γ_{max} is independent of pressure over a wide range at low pressures. Temperature dependence of γ_{max} involves Δf, kT, N, and m. For a diatomic or linear molecule Δf is very nearly proportional to $\frac{1}{T}$ which means that

$$(10) \qquad \gamma_{max} \propto \frac{1}{T^2}$$

and thus

$$(11) \qquad \frac{\Delta\gamma_{max}}{\gamma_{max}} \cong \frac{-2\Delta T}{T}.$$

Thus the percentage change in γ_{max} is seen to be equal in magnitude to twice the percentage change in temperature. For a reasonable temperature change this variation in absorption coefficient can be quite small. High pressure conditions are assumed to become important when the number of collisions involving more than two molecules becomes significant. In such cases the line width is no longer proportional to pressure since the effective number of collisions undergone by one molecule is not simply proportional to the density of the molecules. High pressure may occur as low as 1/2 atmosphere for molecules with large collision diameters such as NH_3. However, low pressure conditions may still exist at 1 atmosphere for other gases such as O_2 which have very small collision diameters.

Lambert's law states that each layer of material of equal thickness absorbs an equal fraction of the radiation which traverses it. From Lambert's law is derived the exponential decrease in intensity given by

$$I = I_o e^{-\gamma x} \tag{12}$$

where γ is the propagation constant or absorption coefficient. In optical spectra departures from Lambert's law are usually associated with polychromatic radiation where individual components are absorbed at different rates. In the microwave region, however, Lambert's law may even break down for monochromatic radiation because of saturation effects. The intensity of radiation can be made so large that absorbing molecules

of a gas cannot get rid of the absorbed energy rapidly enough and γ becomes dependent on the intensity of the radiation. A derivation of γ for this case gives

$$(13)\quad \gamma = \frac{8\pi^2 n_o}{3ckT}\left|\mu_{01}\right|^2 f^2 \left[\frac{\frac{1}{2\pi\tau}}{(f-f_r)^2+\left(\frac{1}{2\pi\tau}\right)^2+\frac{8\pi^2 t}{3ch}\left|\mu_{01}\right|^2 fI\left(\frac{1}{2\pi\tau}\right)}\right]$$

where h = Planck's Constant,

n_o = number of molecules in lower energy state per cm^3,

and $\frac{1}{t}$ = probability per sec. of a molecular transition in state.

Thus as a result of saturation at low pressures, γ is decreased at all frequencies. The most notable effects occur, of course, near the peak absorption at $f=f_r$. The line shape is altered only in that the maximum intensity is decreased by the factor

$$(14)\quad \frac{1}{1+\frac{8\pi^2\left|\mu_{01}\right|^2 fIt\,(2\pi\tau)}{3ch}}$$

and the half bandwidth increased by the factor

$$(15)\quad \left[1+\frac{8\pi^2\left|\mu_{01}\right|^2 fIt2\pi\tau}{3ch}\right]^{\frac{1}{2}}.$$

At high pressures, saturation is generally unobservable. Saturation is considered to become significant when

$$(16) \qquad \frac{8\pi^2 \left|\mu_{01}\right|^2 f I t 2\pi\tau}{3ch} \cong 1$$

Although broadening of the spectral line does occur because of molecular collisions with the cavity walls, this effect plus the doppler broadening effect are normally much less than the pressure broadening effect. Ordinarily a non-polar gas does not absorb microwaves, however it is possible that during collisions some dipole moment may exist. Such a pressure dependent absorption has been found for CO_2.

A somewhat specialized technique to which microwave spectroscopy seems well adapted is the continuous monitoring of various constitutents in a mixture of gases. One could, for instance, monitor the concentration or partial pressure of O_2 in expired air by passing the respiratory gas through the sampling cavity of a microwave spectrometer. Changes in concentration could be very easily and sensitively detected, since the spectrometer itself would be under fixed adjustments and conditions. Furthermore, these changes could be quite rapidly recorded or controlled by the output of the spectrometer. In order to eliminate the effects on spectrometer output due to possible fluctuations in klystron output power, a bridge system could be used with one arm of the bridge containing the absorption cell through which gas is being flowed, and the other arm involving the reference cell. A cavity cell type of instrument is especially useful where the intensity of a particular

absorption line is to be measured over extended periods of time.

For a gaseous mixture of n components, the fractional abundance of one of the components is given by

$$(17) \qquad x_i \propto \gamma_{max} \sum_{j=1}^{n} x_j \frac{\Delta f_{ij}}{P}$$

where x_i = fractional abundance

γ_{max} = maximum absorption due to the i^{th} component

Δf_{ij} = half width of the absorption line of molecule i in the presence of an almost pure sample of molecule j

and P = total pressure

Usually for a mixture of more than two gases, the various values of line width parameters $\frac{\Delta f_{ij}}{P}$ will not be known and thus one usually assumes that γ_{max} is proportional to the fractional abundance or one compares γ_{max} of the unknown sample with values for known mixtures which are similar to it in composition.

REVIEW OF LITERATURE

The two most important topics in the literature that are of special interest in this study are measurement systems using sampling cavities and the cavities themselves. The most important items previously reported in the literature in both of these areas are reviewed in the next two sections.

Systems Using Sampling Cavities

Microwave refractometers have played an important role in tropospheric radio propagation research and in the basic studies of the dielectric properties of gaseous media since their introduction. One of the first successful recording refractometers was reported by Birnbaum (2) in the Review of Scientific Instruments in 1950. This particular instrument utilizes two transmission type cavities in a bridge arrangement excited by a sweep-frequency Klystron. A block diagram of this unit is shown in Figure 1.

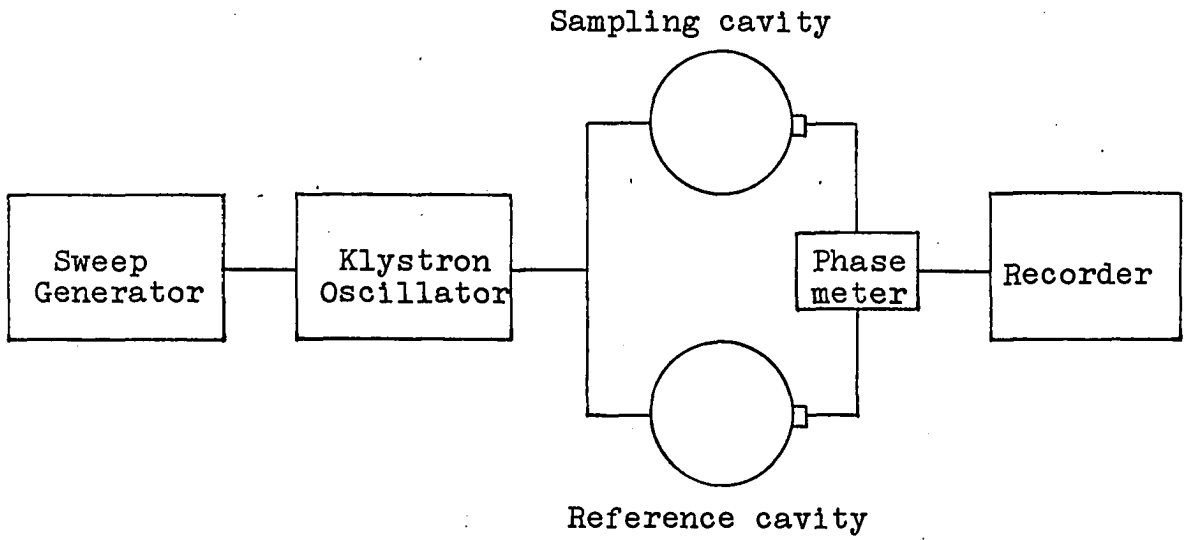

Fig. 1. Diagram of a recording, microwave refractometer

In operation, the Klystron source is caused to sweep in frequency through the resonant point of the cavity and the time difference between the peak point response for the two cavities is measured. This quantity has been shown to be a measure of the refractivity of the sampled medium. The accuracy of this device is dependent upon its ability to maintain a linear sweep and is further limited in accuracy and response time by the phase detector circuitry. Another type of refractometer of interest was reported by Vetter (24) in 1962. This device virtually eliminates the dependence of the refractometer on electronic characteristics of the source and detector circuitry and shifts the limitation to the cavities themselves. A block diagram of this system is shown in Figure 2.

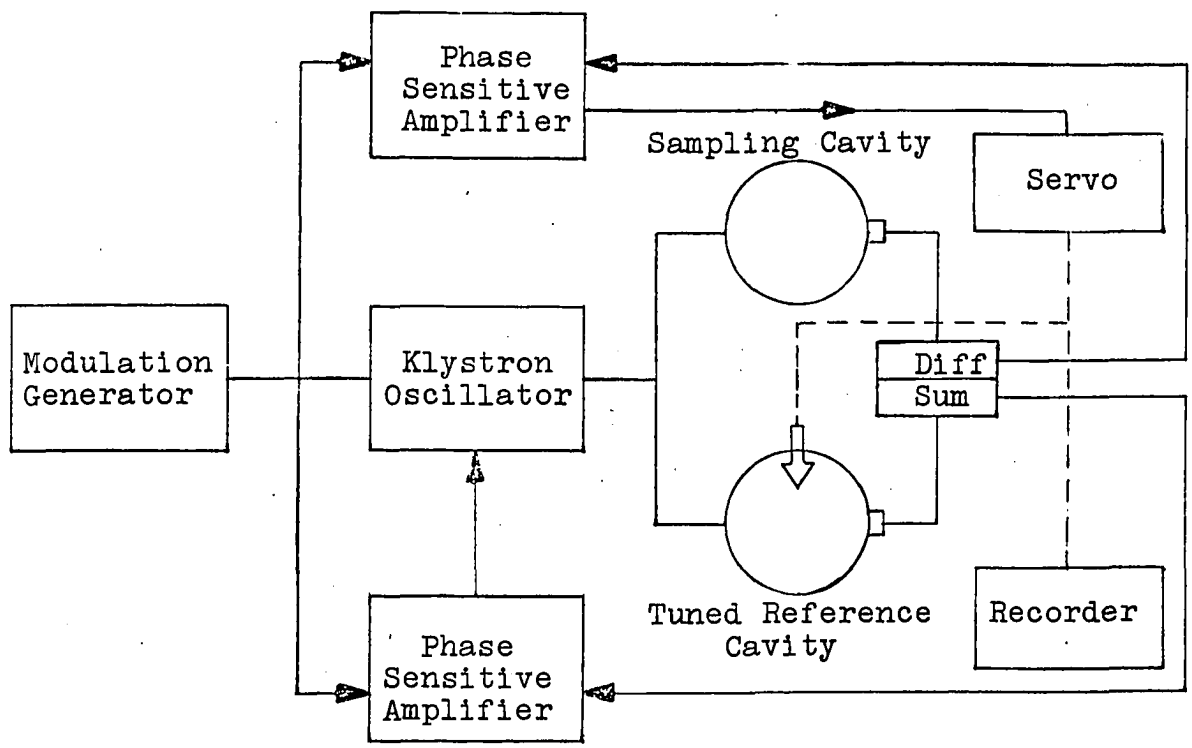

Fig. 2. Block diagram of a Vetter type refractometer

The tunable, sealed reference cavity and the sampling cavity are excited by a single Klystron. The voltages from the cavity detectors are combined to provide outputs of the sum of these voltages and their difference. The sum is used to drive the phase-sensitive amplifier which causes the Klystron frequency to track the resonant frequency of the cavities. The difference voltage is used to drive the second phase-sensitive amplifier which controls the servo that tunes the reference cavity to the resonant frequency of the sampling cavity. The major improvement over the type previously mentioned is the incorporation of the Klystron in a feedback loop and the use of a servo-tuned reference cavity. The response of this device is quite slow, but its absolute accuracy is much better than the type shown in Figure 1. The typical type of sampling cavity used in this instrument is similar to that shown in Figure 4.

Microwave cavity spectrometers have played an important role in the measurement of absorption spectra of various gaseous media. This has led to their use in quantitative gas analysis devices. Typical instruments of this type are shown in block diagram form in Figure 3.

The operation of these instruments rest on the fact that microwave absorption can be detected by its effect on the change in quality factor (Q) of the cavity or by the change in the magnitude of the peak transmission. These changes are shown either by a decrease in the relative amplitude of a wave

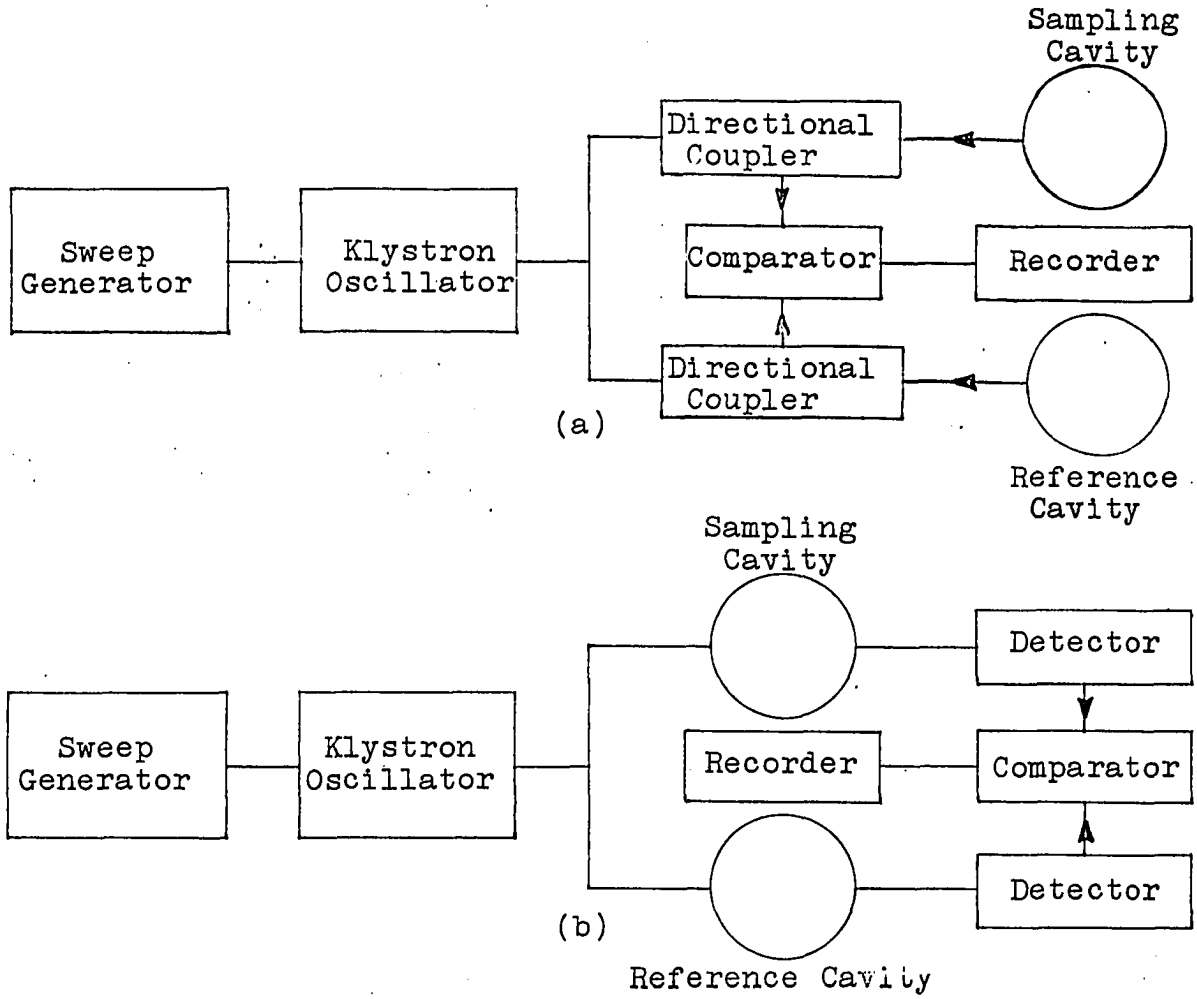

Fig. 3. Block diagrams for microwave cavity spectrometers

(a) Reflection type

(b) Transmission type

transmitted through the cavity or reflected from the cavity input into the waveguide or transmission line coupled to it. If the absorption line is sharper than the cavity response curve it may be displayed by sweeping a microwave oscillator connected to the cavity through the frequency range of the cavity response curve. The maximum or peak absorption is obtained from the difference in the absorption dip with and without the

absorber. This is best used with gases at low pressures where the spectral lines are well separated and narrow in frequency spread. Very wide lines, as in gases at high pressures, can be measured by noting the change in the Q of the cavity at resonance or by simply noting the change in the magnitude of the maximum response of the cavity transmission characteristic. If only one cavity is used then the absorber must either be removed physically or removed by a suitable electromagnetic means as in the Stark spectrograph. Most generally two cavities are used in a bridge type circuit so that removal of the absorber in the sampling cavity is not necessary.

Since a sweep frequency mode is usually used in these instruments, it is usually desirable to make the Q as high as possible for sensitivity reasons, but the cavity bandwidth must be kept greater than the bandwidth of the absorption line so that the maximum absorption can be readily observed and measured.

Microwave Sampling Cavities

A typical sampling cavity of the type presently being used in various microwave instruments is shown in Figure 4. This unit is a transmission type with openings or sampling holes located in the end walls. The ratio of open to closed cavity area is definitely limited in this type of unit because the holes are located in a position that will adversely affect the normal current flow in the end plates for the TE_{onp} type of mode. Cavities of this general type are used in both the Vetter (24) and Birnbaum (2) instruments as well as the various microwave spectrometers.

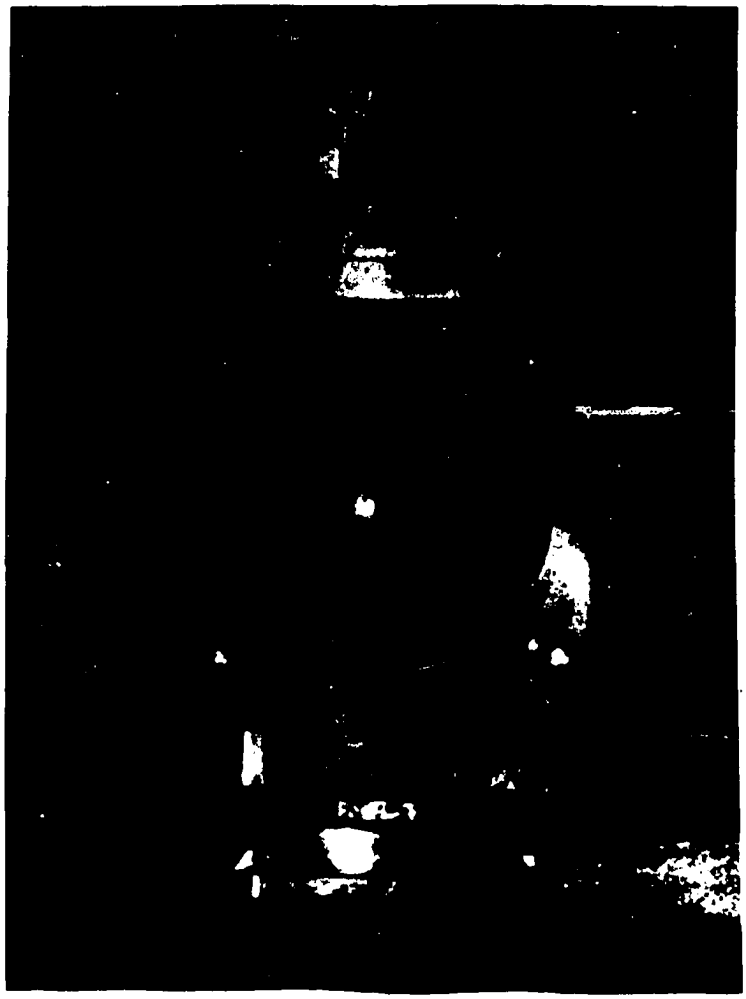

Fig. 4. A typical microwave sampling cavity

THEORETICAL ANALYSIS

Analysis Techniques for Periodic Structures

There are several different theoretical methods that have been used in the literature in the analysis of various periodic microwave structures which appear to have possible application in this study. One is the field approach where one applies Floquet's theorem and Fourier series analysis to arrive at the electromagnetic fields of interest in terms of the so-called space harmonics. In this process a condition equation is derived and must be solved in order to obtain β_o for the waveguide structure or the resonant frequency (f_r) for a cavity structure. The space harmonics can then be computed and used in the determination of Q_o and other quantities of interest. This type of approach has been very successfully used in the analysis of the helical type structures by Sensiper (20) and others. However, in their studies they were interested in space harmonics which have phase velocities less than the speed of light so that electromagnetic fields of a particular space harmonic could be made to interact with an electron beam as in a traveling wave tube. In our study the predominant space harmonic will have a phase velocity greater than the speed of light. It turns out in this case that a somewhat different condition equation will be obtained than was obtained for a tape ring structure by Sensiper (20).

Another possible method for periodic structure analysis is the so-called filter circuit, or equivalent circuit approach. This analysis technique is hard to apply to the problem at hand because the periodic obstacles must be representable by a simple shunt element not only individually, but also when placed in a waveguide in order to obtain a solution for the field components with any accuracy. In other words, these obstacles must be far enough apart so that there is no interaction between them. The results of a filter circuit analysis usually give β_o, pass-band frequencies, and interaction impedances for the space harmonics.

Several other methods of analysis were considered including the perturbational, variational, and coupled mode types. It was found, however, that the field approach was superior for the purposes of this paper. Thus the field approach is applied in the next section in order to determine the electromagnetic fields in a spaced-ring, sampling cavity.

Space Harmonics

A drawing of the particular spaced-ring, cylindrical cavity to be analyzed is shown in Figure 5. Pictures of the experimental units are shown in Figures 17, 18 and 19. This unit consists of five identical sections of length L with rings of thickness δ and open space L-δ. The spacers and holding screws are made of insulative materials which have dielectric constants close to that of free space. Since the

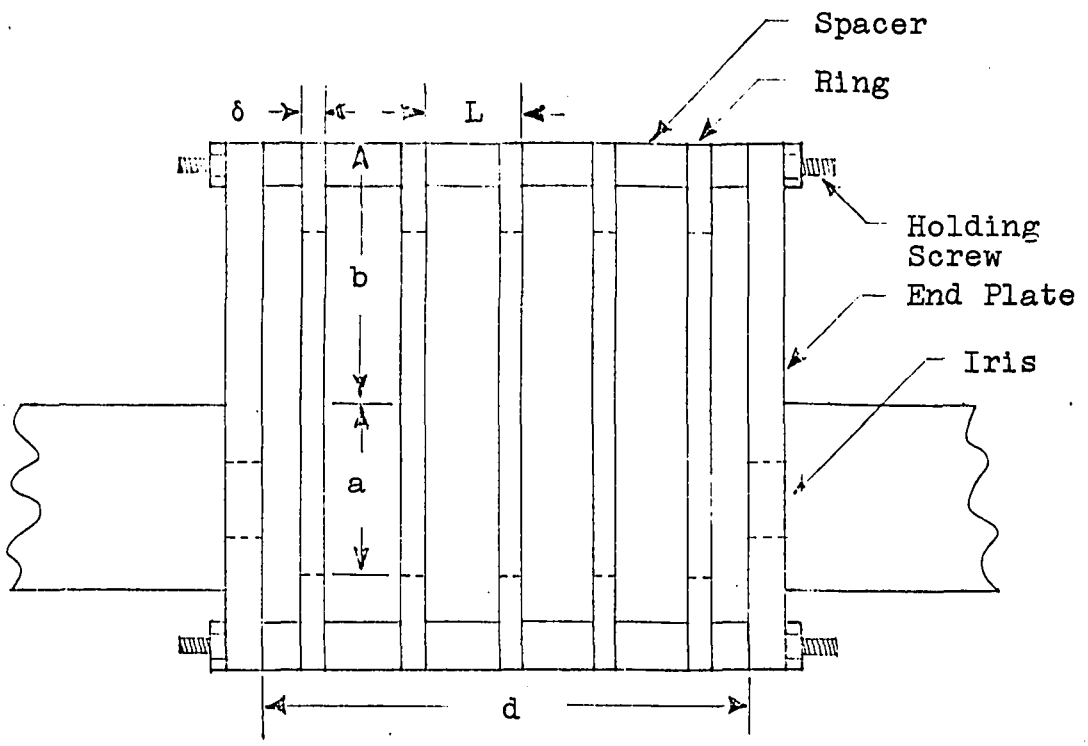

Fig. 5. A spaced-ring, transmission type sampling cavity

determination of the electromagnetic fields within any region is dependent upon one's ability to solve explicitly Maxwell's equation in a coordinate system appropriate to the region and to the boundary conditions, several assumptions are needed to facilitate the analysis using the space harmonic approach. The validity of these assumptions for this analysis will be considered later when the experimental results are discussed.

(a) The fields inside and outside the cavity are

assumed to be the same as for an infinite structure of the same type where the field is zero at z = 0 and z = d for all r.

(b) All modes except the TE_{01p} modes are attenuated to such an extent that their effect on Q_o and f_r may be neglected.

(c) Effects of the source and coupling iris on fields in the cavity can be neglected.

(d) Field components of interest are assumed to have no φ dependence.

The first assumption neglects all end effects and assumes that the currents in the end walls of the cavity are the image currents for the fields of an infinite structure. The fact that the $\vec{E}$ field is not forced to zero at the ends outside the cavity is also neglected.

Because of its general usefulness and application to this problem Floquet's Theorem will be presented here where this presentation is after that in Watkins (25). It states that, "For a given mode of propagation at a given frequency the fields in a periodic structure at one cross-section differ from those one period away only by a complex constant." The Theorem is true whether the structure contains loss or not so long as it is periodic. The proof of the theorem lies in the fact that when the structure having infinite length is displaced along its axis one period, it cannot be distinguished from

its original self. To prove this let us write the field solution as

$$(18) \qquad \vec{\xi}(x,y,z,t) = E'(x,y,z)\ \epsilon^{-\gamma z}\ \epsilon^{jwt}$$

where $E'(x,y,z)\ \epsilon^{-\gamma z}$

is periodic in z with period L. Let $\vec{\xi}_1$ be the field at $z = z_1$ and $\vec{\xi}_2$ be field at $z = z_2$. Then we can write

$$(19) \qquad \vec{\xi}_1 = E'(x,y,z_1)\ \epsilon^{-\gamma z_1}\ \epsilon^{jwt}$$

and

$$(20) \qquad \vec{\xi}_2 = E'(x,y,z_2)\ \epsilon^{-\gamma z_2}\ \epsilon^{jwt}$$

where $z_2 = z_1 + L$ and $E'(x,y,z_2) = E'(x,y,z_1 + L)$.

Thus

$$(21) \qquad \vec{\xi}_1 = E'(x,y,z_1)\ \epsilon^{-\gamma z_1}\ \epsilon^{jwt}$$

and

$$(22) \qquad \vec{\xi}_2 = E'(x,y,z_1 + L)\ \epsilon^{-\gamma(z_1 + L)}\ \epsilon^{jwt}$$

so

$$(23) \qquad \vec{\xi}_2 = \vec{\xi}_1 \epsilon^{-\gamma L}$$

In order to use this theorem we expand the field $E'(x,y,z)\epsilon^{-\gamma z}$ into its Fourier series. Thus we let

$$(24) \quad E'(x,y,z)\ \epsilon^{-\gamma z} = \sum_{\text{all } n} E_n(x,y)\ \epsilon^{-j\frac{2\pi n}{L}z}\ \epsilon^{-\gamma z}$$

and then to find $E_n(x,y)$ we multiply both sides by $\epsilon^{j(\frac{-2\pi n}{L})z + \gamma z}$ and integrate both sides from $z = z_1$ to $z = z_1 + L$. The result is given by

$$(25) \quad E_n(x,y) = \frac{1}{L}\int_{z_1}^{z_1+L} (E_{(x,y,z)}\epsilon^{-\gamma z})\ \epsilon^{(\gamma + j\frac{2\pi n}{L})z}\, dz.$$

This expression can be used to compute the various space harmonics $E_n(x,y)$. The nth term of the series in Equation 24 is called the nth space-harmonic. If the propagation constant $\gamma = j\beta_o$ then the phase constant for the nth harmonic is given by

$$(26) \quad \beta_n = \beta_o + \frac{2\pi n}{L}$$

and thus the phase velocity for the nth harmonic becomes

$$(27) \quad v_n = \omega/\beta_n.$$

In some cases an ω-β diagram is of interest. There are a number of ways to determine the ω-β diagram for a specific

structure. The most common method is to measure the resonant frequencies of a cavity made up of several sections of the waveguide. A typical ω-β plot for a five element cavity is given below in Figure 6.

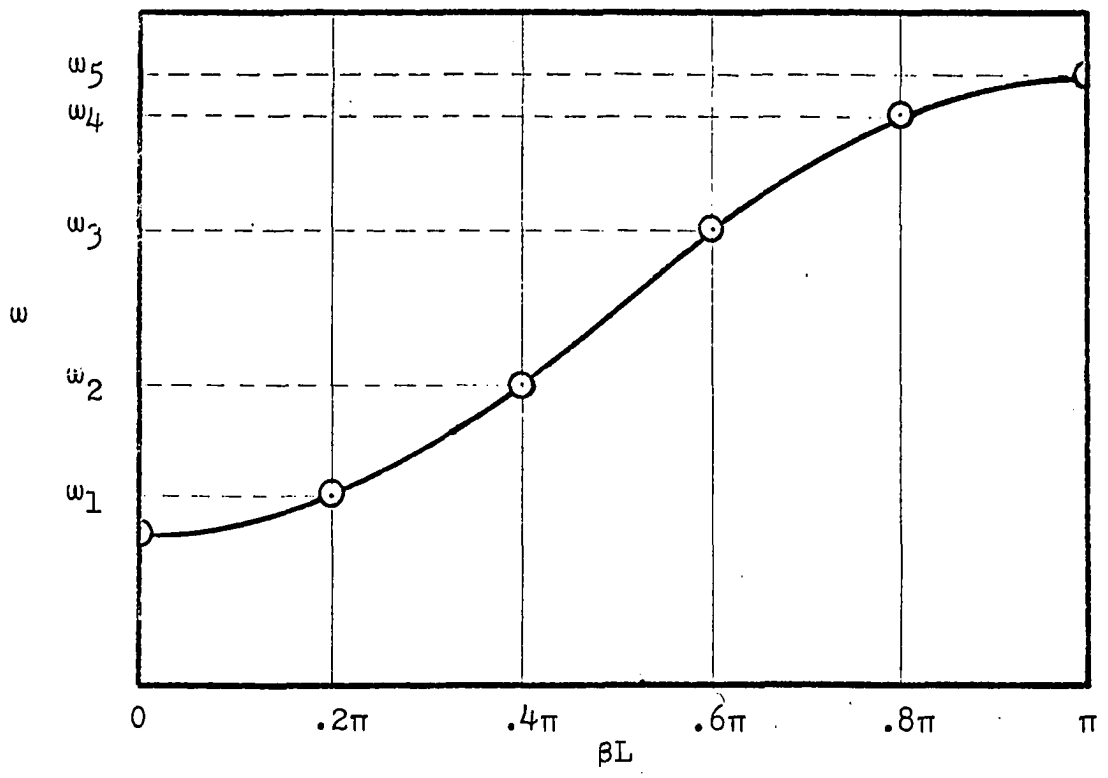

Fig. 6. ω-β diagram for a five element periodic structure

There will be five different resonant frequencies as shown for the zero order space harmonic. They will obviously occur when $\beta L = \pi/5, 2\pi/5, 3\pi/5, 4\pi/5$, and π. Such a diagram can be drawn for the nth harmonic noting that $\beta_n = \beta_o + \frac{2\pi n}{L}$ and that ω is an even function of β.

In the analysis of the structure being considered we seek the proper expressions for the resonant frequency f_r and

unloaded quality factor for the cavity shown in Figure 5 in terms of the ratio δ/L and other important parameters. In order to accomplish this the method of space-harmonics will be used. Neglecting the effects of the source, the homogenous partial differential equation which must be solved is given by

$$(28) \quad \nabla^2 H_z + k^2 H_z = 0$$

where $k^2 = \omega^2 \mu\epsilon$. This equation is derived from Maxwell's equation with time dependence ϵ^{jwt} assumed. Let the solution to Equation 28 in terms of cylindrical coordinates be given by

$$(29) \quad H_z \triangleq H_z'(r,\varphi,z)\ \epsilon^{-\gamma z}$$

where γ is the propagation constant in the +z direction and H_z is periodic of period L. Now expand this solution in terms of a Fourier Series in order to meet the periodic boundary conditions in z at r = a. Thus

$$(30) \quad H_z = H_z'(r,\varphi,z)\ \epsilon^{-\gamma n} = \sum_n H_{nz}(r,\varphi)\ \epsilon^{-\gamma z}\ \epsilon^{-j\frac{2\pi n}{L}z}$$

where

$$(31) \quad H_{nz} = \frac{1}{L} \int_{z_1}^{z_1+L} \left[H_z'(r,\varphi,z)\epsilon^{-\gamma z}\right]\ \epsilon^{\gamma z}\epsilon^{j\frac{2\pi n}{L}z}\ dz.$$

If we let $\gamma = j\beta_o$ and put the assumed solution back into Equation 28 we find that each of the n space harmonics must satisfy the equation

(32) $\nabla_t^2 H_{nz} - \tau_n^2 H_{nz} = 0$

where $\tau_n^2 = \beta_n^2 - k^2$.

The general boundary conditions that must be met in this problem require that the fields be finite at z = o and approach zero as $r \longrightarrow \infty$.

Considering these two general boundary conditions the restricted general solutions for H_z^i inside and H_z^o outside the guide can be written as

(33) $$H_z^i = \epsilon^{-j\beta_o z} \sum_n A_n^i I_o(\tau_n r) \epsilon^{-j\frac{2\pi n}{L}z}$$

and

(34) $$H_z^o = \epsilon^{-j\beta_o z} \sum_n A_n^o K_o(\tau_n r) \epsilon^{-j\frac{2\pi n}{L}z}$$

where $I_o(\tau_n r)$ and $K_o(\tau_n r)$ are zero order modified Bessel functions of the first and second kind, respectively. Now using the fact that

(35) $$E_\varphi = -\frac{j\omega\mu}{\tau_n^2}\left[\frac{\partial H_z}{\partial r}\right]$$ we can show that

(36) $$E_\varphi^i = -j\omega\mu \epsilon^{-j\beta_o z} \sum_n \frac{A_n^i}{\tau_n} I_1(\tau_n r)\epsilon^{-j\frac{2\pi n}{L}z}$$

and

$$(37) \quad E_{\varphi}^{o} = j\omega\mu \; \epsilon^{-j\beta_o z} \sum_n \frac{A_n^o}{\tau_n} K_1(\tau_n r) \; \epsilon^{-j\frac{2\pi n}{L}z}$$

also H_r is non-zero in this case and is given by the equation

$$(38) \quad H_r = \frac{-j\beta_o}{\tau_n^2} \left[\frac{\partial H_z}{\partial r} \right] \qquad \text{which yields}$$

$$(39) \quad H_r^i = -j\beta_o \; \epsilon^{-j\beta_o z} \sum_n \frac{A_n^i}{\tau_n} I_1(\tau_n r) \; \epsilon^{-j\frac{2\pi n}{L}z}$$

and

$$(40) \quad H_r^o = j\beta_o \; \epsilon^{-j\beta_o z} \sum_n \frac{A_n^o}{\tau_n} K_1(\tau_n r) \; \epsilon^{-j\frac{2\pi n}{L}z}$$

All other field components are zero.

The procedure now is to assume the form of the current density on the rings at r = a and expand this into a Fourier series of space-harmonics. Then the boundary conditions are applied. The boundary conditions which apply to the problem at hand are as follows:

(a) The tangential $\vec{E}$ field must be continuous at r = a for all φ and z.

(b) The discontinuity in the tangential $\vec{H}$ field at r = a is equal to the total surface current density.

From (a) we can write that

$$(41) \quad E_{\varphi}^{i}\ (r=a) = E_{\varphi}^{o}\ (r=a)$$

and from (b) we get that

$$(42) \quad J_{\varphi}\ (r=a) = \vec{n} \times (H_z^o - H_z^i)_{r=a} \cdot \vec{a}_z = \vec{a}_{\varphi}(H_z^i - H_z^o)_{r=a}$$

or

$$(43) \quad \left|J_{\varphi}\right|(r=a) = \left|(H_z^i - H_z^o)\right|_{r=a}.$$

Note here that we are letting the superscript (i) refer to field components inside the guide structure and (o) superscript refer to field components outside the guide.

From the above equations it becomes obvious that it is also possible to assume a periodic surface current density J_{φ} at r=a and then to express it in a Fourier series of space-harmonics. The equations of interest are then given by

$$(44) \quad J_{\varphi}(r=a) = J_{\varphi}'(r=a)\ \epsilon^{-\gamma z} = \sum_{n} J_{n\varphi}(a,\varphi)\ \epsilon^{-\gamma z}\ \epsilon^{-j\frac{2\pi n}{L}}\ dz$$

and

$$(45) \quad J_{n\varphi}(a,\varphi) = \frac{1}{L}\int_{z_1}^{z_1+L} J_{\varphi}'\ (a,\varphi,z)\ \epsilon^{+\gamma z}\ \ \epsilon^{-\gamma z}\ \epsilon^{j\frac{2\pi n}{L}z}\ dz$$

where $J_{n\varphi}$ is the complex Fourier amplitude of the current density associated with the nth harmonic. In order to use this approach to solve the problem at hand assume a current density

function at r=a. Although it would appear that an incorrect assumption here would be fatal, it turns out that the functional form shown in Figure 7 is sufficiently accurate for most cases. In this paper we will assume the surface current density to have the z - dependence shown in Figure 7.

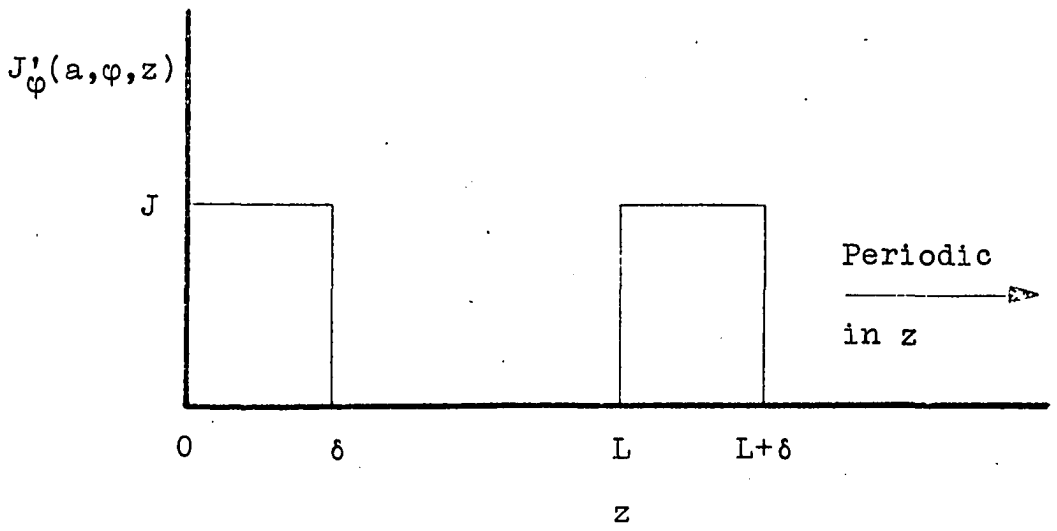

Fig. 7. Assumed current distribution on rings at r=a

Using this function in the integral of Equation 45 we get

$$(46) \qquad J_{n\varphi(r=a)} = Je^{j\frac{\beta_n \delta}{2}} \left[\frac{\sin \frac{\beta_n \delta}{L}}{\frac{\beta_n \delta}{L}} \right].$$

In order to effect a solution one further condition equation relating the magnitudes of the space harmonics A_n^i and A_n^o is needed. This condition can be stated in three different ways. One is called the thin ring case where $\delta << L$ and

$$(47) \qquad E_\varphi^o(r=a) = E_\varphi^i(r=a) \qquad \text{for} \qquad z = mL + \delta/2.$$

This says that the electric field is constrained to be zero only at the center of the rings. This is accurate only for very thin rings. The next is referred to as the wide ring or narrow gap case where $L-\delta \ll L$. In this case we set

$$(48) \quad H_z^o(r=a) = H_z^i(r=a) \qquad \text{at} \qquad z = (mL - \frac{L-\delta}{2}).$$

A more accurate condition equation than either of the above is given by

$$(49) \quad 2\pi a \int_o^L \left(E_\varphi(r=a)\right) \cdot \left(J_\varphi^*(r=a)\right) \, dz = 0.$$

A more stringent requirement expressed as

$$(50) \quad (E_\varphi(r=a)) \cdot (J_\varphi^*(r=a)) = 0 \qquad \text{for all } z \text{ may also be used.}$$

Condition Equation 49 will be used here. It can be seen to be correct since the electric field is zero on the ring surface and the current density is zero in the gap. Although it would be desirable to use the boundary condition in Equation 50, it turns out that Equation 49 is much easier to apply. The justification for using Equation 49 rests on the fact that it minimizes the error in matching the electric field for the assumed current distribution by making the average error equal to zero.

There are two cases to be considered. First, let us take

the case where the wall thickness (b-a) is approximately zero. A finite wall thickness will be considered later. The boundary conditions are then expressible in terms of the equations

$$(51) \quad E_z^i = E_z^o,$$

$$(52) \quad H_z^i - H_z^o = J_\varphi,$$

and

$$(53) \quad \int_o^L (E_\varphi)(J_\varphi^*)\, dz = 0$$

Using Equations 51 and 52 the condition equations obtained are

$$(54) \quad A_n^i\, I_o(\tau_n a) - A_n^o\, K_o(\tau_n a) = \frac{J\delta}{L} \left[\frac{\sin \frac{\beta_n \delta}{L}}{\frac{\beta_n \delta}{L}} \right]$$

and

$$(55) \quad A_n^i\, I_1(\tau_n a) + A_n^o\, K_1(\tau_n a) = 0$$

From these two equations we can write that

$$(56) \quad A_n^i = \frac{\frac{J\delta}{L}\, K_1(\tau_n a) \left[\frac{\sin \frac{\beta_n \delta}{L}}{\frac{\beta_n \delta}{L}} \right]}{I_o(\tau_n a)\, K_1(\tau_n a) + K_o(\tau_n a)\, I_1(\tau_n a)}$$

and

$$(57) \qquad A_n^o = \frac{\frac{J\delta}{L} I_1(\tau_n a) \left[\frac{\sin \frac{\beta_n \delta}{L}}{\frac{\beta_n \delta}{L}}\right]}{I_o(\tau_n a) K_1(\tau_n a) + K_o(\tau_n a) I_1(\tau_n a)}.$$

Using the condition given in Equation 53 we can write that the

$$(58) \qquad \int_o^L -j\omega\mu \left[\sum_n \frac{A_n^i}{\tau_n} I_1(\tau_n a) \epsilon^{-j\beta_n z}\right] \cdot \left[\sum_m \frac{J\delta}{L} \frac{\sin \frac{\beta_m \delta}{z}}{\frac{\beta_m \delta}{z}} \epsilon^{j\beta_m z}\right] dz = 0.$$

For $m \neq n$ Equation 58 is equal to zero and thus Equation 58 can be written as the

$$(59) \qquad \int_o^L -j\omega\mu \sum_n \frac{A_n^i J\delta}{L\tau_n} I_1(\tau_n a) \left[\frac{\sin \frac{\beta_n \delta}{L}}{\frac{\beta_n \delta}{L}}\right] dz = 0.$$

Upon integration of Equation 59 one obtains Equation 60.

$$(60) \qquad \sum_n \frac{A_n^i}{\tau_n} I_1(\tau_n a) \frac{\sin \frac{\beta_n \delta}{L}}{\frac{\beta_n \delta}{L}} = 0$$

Now substituting for A_n^i from Equation 56 we get that the

$$(61) \qquad \sum_n \frac{K_1(\tau_n a)\, I_1(\tau_n a) \left[\dfrac{\sin \dfrac{\beta_n \delta}{L}}{\dfrac{\beta_n \delta}{L}}\right]^2}{\tau_n (I_o(\tau_n a)\, K_1(\tau_n a) + K_o(\tau_n a)\, I_1(\tau_n a))} = 0.$$

Now since $I_o(\tau_n a)\, K_1(\tau_n a) + K_o(\tau_n a)\, J_1(\tau_n a) = \frac{1}{\tau_n a}$ we can write Equation 61 in the form

$$(62) \qquad \sum_n K_1(\tau_n a)\, I_1(\tau_n a) \left[\frac{\sin \dfrac{\beta_n \delta}{L}}{\dfrac{\beta_n \delta}{L}}\right]^2 = 0.$$

If one examines this last equation one can show that for $\tau_n a$ real all terms are positive real and thus one cannot hope for this summation to be equal to zero. Since our structure is not an infinite one, we can disregard the requirement of no radiation per unit length from the structure which would require an infinite source and look to one or more of the space harmonics to have phase velocities greater than the velocity of light. Let us consider the n=o space harmonic to have this possibility. Then we can write Equation 62 in the form

$$(63) \qquad -I_1(\tau_o a)\, K_1(\tau_o a) = \sum_{n \neq o} I_1(\tau_n a)\, K_1(\tau_n a) \left[\frac{\sin \dfrac{\beta_n \delta}{L}}{\dfrac{\beta_n \delta}{L}}\right]^2$$

where $\tau_n = \sqrt{\beta_n^2 - k^2}$

and $\beta_n = \beta_o + \frac{2\pi n}{L}$.

For the n=o harmonic we assume that $\beta_o < k$ and thus

$$(64) \quad \tau_o = jk_o = j\sqrt{k^2 - \beta_o^2}\,.$$

Now using the identities

$$(65) \quad I_1(u) = j\, J_1(-ju)$$

and

$$(66) \quad K_1(u) = -\pi/2\, H_1^{(2)}(-ju)$$

we get

$$(67) \quad \pi/2 \left[N_1(k_o a)\, J_1(k_o a) + j\, J_1^2(k_o a)\right] = \sum_{n\neq o} I_1(\tau_n a)\, K_1(\tau_n a) \left[\frac{\sin \frac{\beta_n \delta}{L}}{\frac{\beta_n \delta}{L}}\right]^2.$$

Now since the boundary condition on the unperturbed waveguide for the TE_{on} modes requires that $J_1(k_o a) = 0$, we look for an approximate solution to Equation 67 under the assumption that $J_1(k_o a) << N_1(k_o a)$ and that all $\tau_n a$ for $n\neq o$, are positive real. These assumptions reduce the condition equation to that given in Equation 68.

$$(68) \quad \frac{\pi}{2} N_1(k_o a)\, J_1(k_o a) \cong \sum_{n\neq o} I_1(\tau_n a)\, K_1(\tau_n a) \left[\frac{\sin \frac{\beta_n \delta}{L}}{\frac{\beta_n \delta}{L}}\right]^2$$

The convergence of the summation in Equation 67 is discussed in Appendix C. For the large argument form which is sufficiently valid where $\tau_n a$ for $n \neq o$ is greater than 10 we get

$$(69) \quad \frac{\pi}{2} J_1(k_o a)\, N_1(k_o a) \cong \sum_{n \neq o} \left(\frac{1}{2\tau_n a}\right) \left[\frac{\sin \frac{\beta_n \delta}{L}}{\frac{\beta_n \delta}{L}}\right]^2$$

where for $n \neq o$

$$(70) \quad \tau_n a = \sqrt{\left(\beta_o + \frac{2\pi n}{L}\right)^2 a^2 - k^2 a^2}$$

and for $n = o$

$$(71) \quad \tau_o a = j k_o a = \sqrt{j^2 k^2 a^2 - \beta_o^2 a^2} \quad .$$

It is now assumed that the foregoing derivation for an infinite waveguide structure is also valid for a cavity made of the same elements. For the cavity case we require $\beta_o = p\pi/d$ where $p = 1, 2, 3, \ldots$ because of the end plates. The cavity modes of interest are the TE_{01p} types where $k_o a = 3.835$ for the unperturbed cavity for all p. In order to solve for the actual $k_o a$ for a periodic structure we use an iterative procedure. First let $k_o a = 3.835$ which is the value for an unperturbed structure. Then calculate $\tau_n a$ using the equation

$$(72) \quad \tau_n a = \left[4\pi^2 m^2 \left(\frac{a}{d}\right)^2 \left(\frac{np}{m} + n^2\right) - k_o^2 a^2\right]^{\frac{1}{2}}$$

where p = number of half wavelengths in cavity length d,

n = index of summation,

d = length of cavity,

and m = number of identical units of length L in length d. Next solve for a new $k_o a$ using Equation 69. Repeat this procedure until the change in $k_o a$ over one iteration is sufficiently small. Now take the last value of $k_o a$ from this iterative computation and use it to solve for the resonant frequency which is given by the expression

$$(73) \quad f_{r_{01p}} = \frac{1}{2\pi a\sqrt{\mu\epsilon}}\sqrt{(k_o a)^2 + (\frac{\pi p a}{d})^2}$$

Resonant Frequency Determination

The ratio of the resonant frequency for the spaced-ring cavity to the resonant frequency of a closed cavity is given by

$$(74) \quad \frac{f_{r_{01p}}\ (\text{open})}{f_{r_{01p}}\ (\text{closed})} = \sqrt{\frac{k_o^2 a^2 + (\frac{\pi p a}{d})^2}{(\tau'_{01})^2 + (\frac{\pi p a}{d})^2}}$$

In order to determine the validity of this development resonant frequency measurements were made on a constant length cavity for various values of δ/L. The cavities used in these experiments are shown in Figure 18, 19, and 20. The non-varying dimensions of interest are length $d = 3.17 \times 10^{-2}$ meters, radius $a = 2.27 \times 10^{-2}$ meters and wall thickness $(b-a) = .9 \times 10^{-2}$ meters. For definition of dimensions see Figure 5.

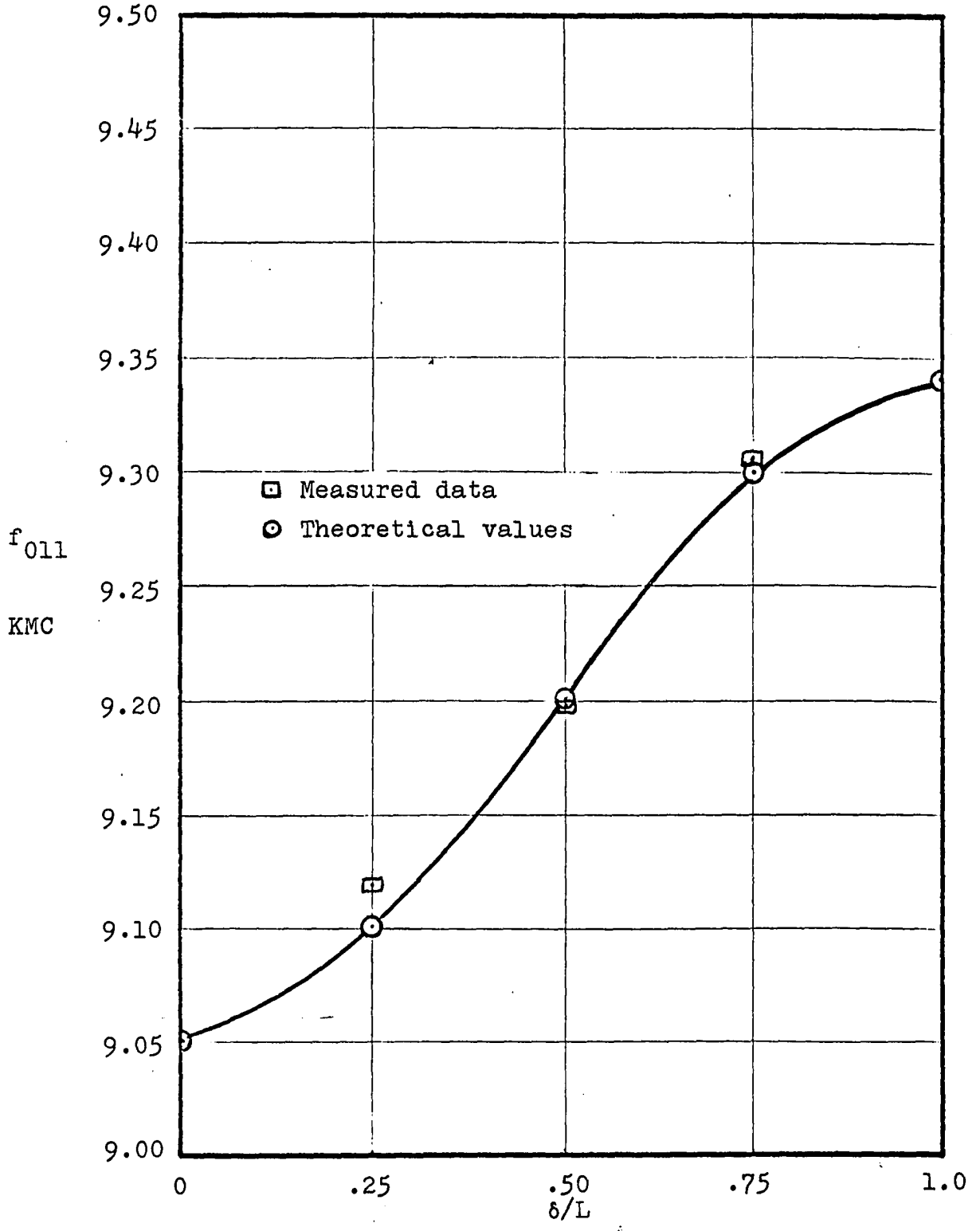

Fig. 8. Cavity resonant frequency f_{011} versus δ/L

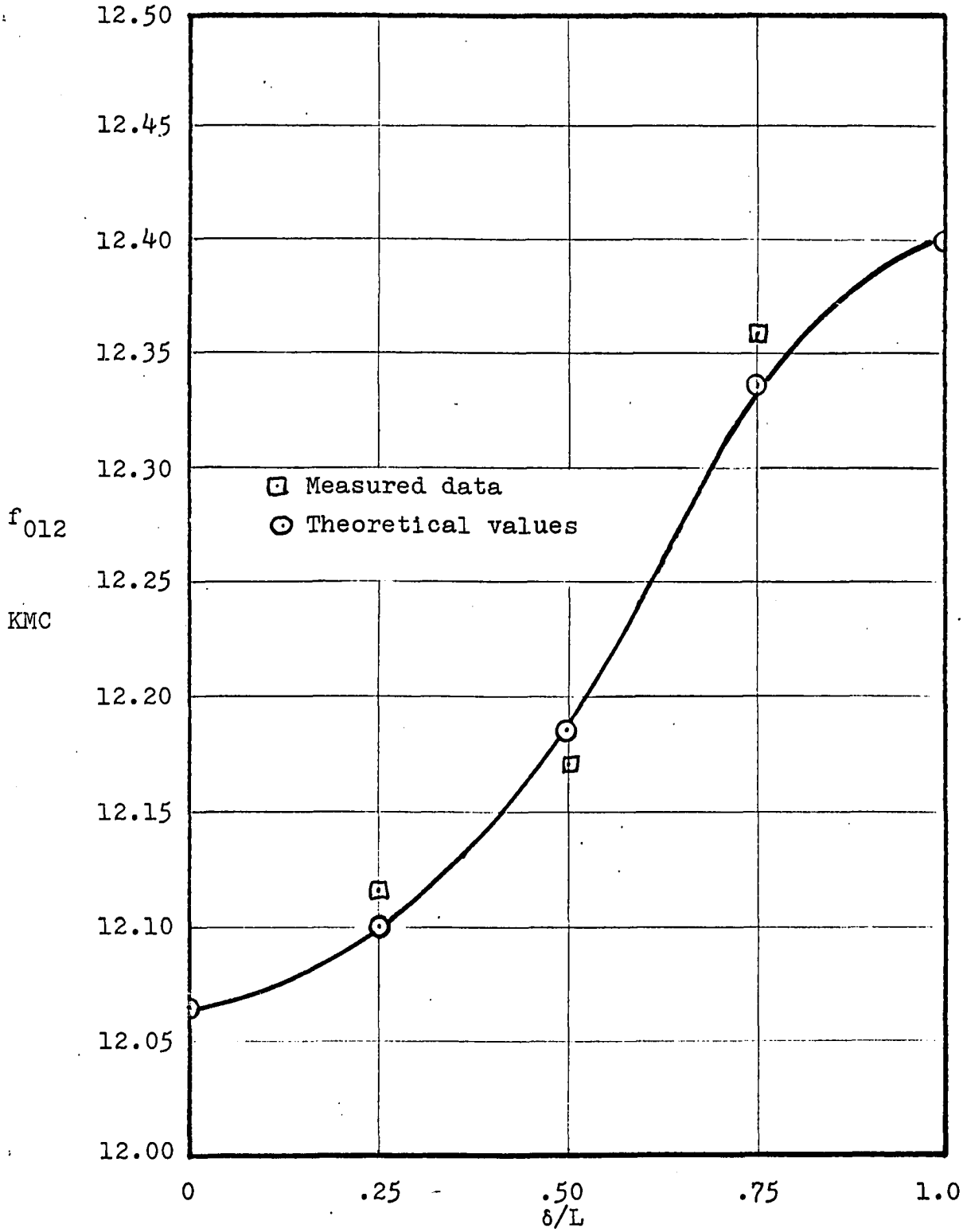

Fig. 9. Cavity resonant frequency f_{012} versus δ/L

Quality Factor Determination

Next we look to the computation of the Q_o of the spaced-ring cavity. This can be accomplished by evaluation of the expression for unloaded quality factor given by the equation

$$(75) \quad Q_o = \frac{\omega U_{max}}{P_T}$$

where U_{max} = maximum energy stored per cycle (joules)

ω = angular frequency (rad/sec)

and P_T = total average power loss (watts).

In order to compute U_{max} we will break the problem into two distinct regions. One inside the cavity and the other outside the cavity. The expressions for these energy terms are given below.

$$(76) \quad U^i_{max} = \frac{1}{2} \int_{V_i} \epsilon \, E^{i\,2}_{\varphi} \, dv$$

$$(77) \quad U^o_{max} = \frac{1}{2} \int_{V_o} \epsilon \, E^{o\,2}_{\varphi} \, dv$$

In order to evaluate these two integrals we will use the fields given by

$$(78) \quad E^o_{\varphi} = j\omega\mu \sum_n \frac{2A^o_n}{\tau_n} K_1(\tau_n r) \sin \beta_n z$$

and

$$(79) \quad E^i_{\varphi} = -j\omega\mu \sum_n \frac{2A^i_n}{\tau_n} I_1(\tau_n r) \sin \beta_n z .$$

Ignoring end effects the maximum energy stored outside the cavity is given by

$$(80) \quad U^{o}_{max} \cong \frac{1}{2} \int_{o}^{d} \int_{a}^{\infty} \epsilon \left| E^{o}_{\varphi} \right|^2 2\pi r dr dz \qquad n \neq o$$

and inside the cavity by

$$(81) \quad U^{i}_{max} \cong \frac{1}{2} \int_{o}^{d} \int_{o}^{a} \epsilon \left| E^{i}_{\varphi} \right|^2 2\pi r dr dz$$

All terms in the last two equations which result from the double summation resulting from $E^{i}_{\varphi}{}^{2}$ or $E^{o}_{\varphi}{}^{2}$ and where $n \neq m$ result in zero when integrated from zero to d on z. Thus we can write the integrals of Equation 81 in the following form

$$(82) \quad U^{i}_{max} = 4\pi \epsilon \mu^2 \omega^2 \sum_{n} \int_{o}^{d} \int_{o}^{a} \frac{\left| A^{i}_{n} \right|^2}{\tau_n^2} I_1^2(\tau_n r) \sin^2(\beta_n z)\, r dr dz$$

where for the n=o term we get

$$(83) \quad U^{i}_{max}\ (n=o) = 4\pi \epsilon \mu^2 \omega^2 \int_{o}^{d} \int_{o}^{a} \frac{\left| A^{i}_{o} \right|^2}{k_o^2} J_1^2(k_o r) \sin^2(\beta_o z)\, r dr dz$$

since $\tau_o = jk_o$.

For U^{o}_{max} we do not consider the n=o term since it represents radiated power and therefore is a loss term component. The energy stored (max) outside the guide is given by

$$(84) \quad U^{o}_{max} = 4\pi \epsilon \mu^2 \omega^2 \sum_{n \neq o} \int_{o}^{d} \int_{a}^{\infty} \frac{\left| A^{o}_{n} \right|^2}{\tau_n^2} K_1^2(\tau_n r) \sin^2(\beta_n z)\, r dr dz$$

The total energy stored is then given by

$$(85) \quad U_{max} = U^{i}_{max}(n\neq o) + U^{i}_{max}(n=o) + U^{o}_{max}(n\neq o)$$

Now using Equations 56 and 57 Equation 85 reduces to

$$(86) \quad U_{max} = 4\pi\epsilon\mu^2\omega^2 \sum_{n\neq o} \int_o^d \int_o^a \frac{|A^i_n|^2}{\tau_n^2} I_1^2(\tau_n r) \sin^2(\beta_n z)\, r\,dr\,dz$$

$$+ \int_o^d \int_o^a \frac{|A^i_o|^2}{k_o^2} J_1^2(k_o r) \sin^2(\beta_o z)\, r\,dr\,dz$$

$$+ \sum_{n\neq o} \int_o^d \int_a^\infty \frac{|A^o_n|^2}{\tau_n^2} K_1^2(\tau_n a) \sin^2(\beta_n z)\, r\,dr\,dz$$

Evaluating each integral we get the following equation

$$(87) \quad U_{max} = \pi\epsilon\mu^2\omega^2 da^2 \left[\frac{|A^i_o|^2}{k_o^2} \left(J_1^2(k_o a) - J_o(k_o a)\, J_2(k_o a) \right) \right.$$

$$- \sum_{n\neq o} \frac{|A^i_n|^2}{\tau_n^2} \left(I_1'^2(\tau_n a) - \left(1 + \frac{1}{(\tau_n a)^2}\right) I_1^2(\tau_n a) \right)$$

$$\left. + \sum_{n\neq o} \frac{|A^o_n|^2}{\tau_n^2} \left(K_1'^2(\tau_n a) - \left(1 + \frac{1}{(\tau_n a)^2}\right) K_1^2(\tau_n a) \right) \right]$$

Now since

$$(88) \quad |A^o_n|^2 = |A^i_n|^2 \frac{I_1^2(\tau_n a)}{K_1^2(\tau_n a)}$$

from the boundary conditions, we can reduce the two summations above to a single summation so that

$$(89)\quad U_{max} = \pi\epsilon\mu^2\omega^2 da^2 \left[\frac{\left|A_o^i\right|^2}{k_o^2} \left(J_1^2(k_o a) - J_o(k_o a)\, J_2(k_o a) \right) + \sum_{n\neq o} \frac{\left|A_n^i\right|^2}{\tau_n^2} \left(\frac{I_1^2(\tau_n a)\, K_1'^2(\tau_n a) - K_1^2(\tau_n a)\, I_1'^2(\tau_n a)}{K_1^2(\tau_n a)} \right) \right]$$

Now since

$$(90)\quad I_1(z)\, K_1'(z) - I_1'(z)\, K_1(z) = -\frac{1}{z},$$

$$(91)\quad I_1^2(\tau_n a)\, K_1'^2(\tau_n a) - K_1^2(\tau_n a)\, I_1'^2(\tau_n a) = -\frac{1}{\tau_n a} \left(I_1(\tau_n a)\, K_1'(\tau_n a) + K_1(\tau_n a)\, I_1'(\tau_n a) \right),$$

and

$$(92)\quad K_1'(\tau_n a) = \frac{K_1(\tau_n a)}{\tau_n a} - K_2(\tau_n a),$$

the term

$$(93)\quad I_1^2(\tau_n a)\, K_1'^2(\tau_n a) - K_1^2(\tau_n a)\, I_1'^2(\tau_n a) = -\frac{1}{\tau_n a} \left(I_1(\tau_n a) \left(\frac{K_1(\tau_n a)}{\tau_n a} - K_2(\tau_n a) \right) + K_1(\tau_n a) \right).$$

Thus we can write the maximum energy function as

$$(94)\quad U_{max} = \pi\epsilon\mu^2\omega^2 da^2 \left[\frac{\left|A_o^i\right|^2}{k_o^2} \left(J_1^2(k_o a) - J_o(k_o a)\, J_2(k_o a) \right) \right.$$

$$\left(\frac{I_1(\tau_n a)}{\tau_n a} + I_2(\tau_n a)\right) \quad + \sum_{n\neq o} \frac{\left|A_n^i\right|^2}{\tau_n^2}$$

$$\frac{\frac{1}{(\tau_n a)^2}\left[\tau_n a(I_1(\tau_n a)\, K_2(\tau_n a) - I_2(\tau_n a)\, K_1(\tau_n a)) - 2I_1(\tau_n a)K_1(\tau_n a)\right]}{K_1^2(\tau_n a)}$$

Using the large argument form for $I_n(\tau_n a)\, K_n(\tau_n a)$ given by

$$(95) \qquad I_n(\tau_n a)\, K_n(\tau_n a) \longrightarrow \frac{1}{2\tau_n a}$$

$$\tau_n a \longrightarrow \infty$$

for $n\neq o$ Equation 94 can be written as

$$(96) \qquad U_{max} \cong \pi\epsilon\mu^2\omega^2 d a^4 \left[\frac{\left|A_o^i\right|^2}{(ak_o)^2}\left(J_1^2(k_o a) - J_o(k_o a)\, J_2(k_o a)\right)\right.$$

$$\left. - \sum_{n\neq o} \frac{\left|A_n^i\right|^2}{(\tau_n a)^5\, K_1^2(\tau_n a)}\right].$$

For $n\neq o$ we can use the equation

$$(97) \qquad \left|A_n^i\right|^2 = \frac{J^2\delta^2 a^2 \tau_n^2}{L^2}\, K_1^2(\tau_n a)\left[\frac{\sin\frac{\beta_n \delta}{L}}{\frac{\beta_n \delta}{L}}\right]^2$$

and for $n=o$

$$(98) \qquad \left|A_o^i\right|^2 = \frac{J^2\delta^2 a^2 k_o^2 \pi^2}{4L^2}\left(J_1^2(k_o a) + N_1^2(k_o a)\right).$$

Putting Equations 97 and 98 into Equation 96 we get

$$(99)\quad U_{max} \cong \frac{\pi\varepsilon\mu^2\omega^2 d a^4 J^2 \delta^2}{4L^2}\left[\left(J_1^2(k_o a) - J_o(k_o a)\, J_2(k_o a)\right)\right.$$
$$\left.\cdot\left(J_1^2(k_o a) + N_1^2(k_o a) - \sum_{n\neq o}\frac{4}{\pi^2}\left(\frac{1}{\tau_n a}\right)^3\left[\frac{\sin\frac{\beta_n\delta}{L}}{\frac{\beta_n\delta}{L}}\right]^2\right)\right]$$

It turns out for the cases considered that the summation in Equation 99 is negligible compared to the first term so that

$$(100)\quad U_{max} \cong \frac{\pi^3\varepsilon\mu^2\omega^2 d a^4 J^2\delta^2}{4L^2}\left[\left(J_1^2(k_o a) - J_o(k_o a)\, J_2(k_o a)\right)\right.$$
$$\left.\cdot\left(J_1^2(k_o a) + N_1^2(k_o a)\right)\right]$$

This last equation will be utilized in the determination of Q_o for the cavity. Note here that the term neglected above represents the energy stored outside the cavity, and may have to be included if it is not sufficiently small.

The power loss due to radiation is only present in the n=o term outside the guide. The power density in the +r direction is given by

$$(101)\quad P_r = \frac{1}{2}\,\mathrm{Re}\left[E^o_{o\varphi}\, H^{*o}_{oz}\right]$$

and thus the total average power radiated is given by

$$(102)\quad P_{L_{rad}} = \int_o^d P_r\Big|_{r\to\infty} 2\pi r dz$$

or

$$(103)\quad P_{L_{rad}} = \mathrm{Re} \int_o^d \pi E^o_{o\varphi} H^{*o}_{oz}\Big|_{r\to\infty} rdz.$$

Since

$$(104)\quad E^o_{o\varphi} = j\omega\mu \frac{2A^o_o}{\tau_o} K_1(\tau_o r) \sin \beta_o z$$

and

$$(105)\quad H^o_{oz} = 2A^o_o K_o(\tau_o r) \sin \beta_o z$$

where $\tau_o = jk_o$, we can write

$$(106)\quad E^o_{o\varphi} = \omega\mu \frac{2A^o_o}{k_o} (-\pi/2\ H^{(2)}_1(k_o r)) \sin \beta_o z$$

and

$$(107)\quad H^o_{oz} = 2A^o_o\ (-j\ \pi/2\ H^{(2)}_o(k_o r))\ \sin \beta_o z.$$

Now using Equation 103 we get

$$(108)\quad P_{L_{rad}} = \underset{r\to\infty}{\mathrm{Re}} \left[-j \frac{\pi^3 \omega\mu \left|A^o_o\right|^2}{k_o} \int_o^d H^{(2)}_1(k_o r)\ H^{(2)}_o(k^*_o r) \cdot \sin^2(\beta_o z) rdz \right].$$

Now as r approaches ∞

$$(109)\quad H^{(2)}_1(k_o r) \longrightarrow j\sqrt{\frac{2j}{\pi k_o r}}\ \epsilon^{-jk_o r}$$

and

$$(110)\quad H_o^{(2)^*}(k_o r) \longrightarrow \sqrt{\frac{-j2}{\pi k_o r}}\ \epsilon^{jk_o r},$$

then

$$(111)\quad P_{L_{rad}} = \left(\frac{4\pi^2 \omega\mu d a^2 J^2 \delta^2}{4L^2}\right) J_1^2(k_o a).$$

The average power loss in the walls of the guide can be computed using the equation

$$(112)\quad P_{L_{wall}} = \frac{1}{2} \sum_{q=o}^{m-1} \int_{ql}^{ql+\delta} R_s \left|H_z^i\right|^2 (r=a)\ 2\pi a\ dz.$$

Using the fact that

$$(113)\quad \left|H_z^i\right|^2 \cong 4\left|A_o^i\right|^2 J_o^2(k_o a) \sin^2 \beta_o z$$

and neglecting the other space harmonics the integral Equation 112 can be written in the form

$$(114)\quad P_{L_{wall}} \cong \frac{2\pi^3 a^3 R_s J^2 \delta^2 k_o^2}{4L^2} \Big[(J_1^2(k_o a) + N_1^2(k_o a)) \cdot (J_o^2(k_o a) + (J_o^2(k_o a) + N_o^2(k_o a))\,(J_1^2(k_o a))\Big] F(m, \tfrac{\delta}{L})$$

where

$$(115)\quad F(m,\tfrac{\delta}{L}) = m\delta - \sum_{q=o}^{m-1} \frac{d}{2p\pi} \left[\sin\frac{2\pi p(q+\frac{\delta}{L})}{m} - \sin\frac{2\pi pq}{m} \right].$$

It turns out that for a symmetrical unit the summation in Equation 115 is always zero so

$$(116)\quad F(m,\tfrac{\delta}{L}) = m\delta$$

and thus

$$(117)\quad P_{L_{wall}} \cong \frac{2\pi^3 a^3 R_s J^2 \delta^2 k_o^2}{4L^2} \left[(J_1^2(k_o a) + N_1^2(k_o a))\ (J_o^2(k_o a)) + (J_o^2(k_o a) + N_o^2(k_o a))(J_1^2(k_o a)) \right] m\delta$$

In the computation of the end losses as with the wall losses we will consider only the n=o space harmonic component. On this basis then

$$(118)\quad H_r^{i\,2}(z=o) = \frac{4\beta_o^2}{k_o^2} \left|A_o^i\right|^2 J_1^2(k_o r)$$

and

$$(119)\quad P_{L_{ends}} = 2\int_o^a \frac{1}{2} R_s \left|H_r^i\right|^2 (z=o)\ 2\pi r dr.$$

This can be written as

$$(120)\quad P_{L_{ends}} = \frac{8\pi R_s \beta_o^2 \left|A_o^i\right|^2}{k_o^2} \int_o^a r J_1^2(k_o r)\ dr$$

where

$$(121)\quad \left|A_o^i\right|^2 = \frac{J^2 \delta^2 a^2 k_o^2 \pi^2}{4L^2} \left(J_1^2(k_o a) + N_1^2(k_o a)\right)$$

and thus

$$(122)\quad P_{L_{ends}} = \frac{8\pi^3 R_s \beta_o^2 J^2 \delta^2 a^2}{4L^2}\left[\frac{a^2}{2}\left(J_1^2(k_o a) - J_o(k_o a)\, J_2(k_o a)\right)\right.$$

$$\left.\cdot\left(J_1^2(k_o a) + N_1^2(k_o a)\right)\right].$$

The equation for end losses in the cavity is thus given by

$$(123)\quad P_{L_{ends}} = \frac{4\pi^3 R_s \beta_o^2 J^2 \delta^2 a^4}{4L^2}\left[\left(J_1^2(k_o a) - J_o(k_o a)\, J_2(k_o a)\right)\right.$$

$$\left.\cdot\left(J_1^2(k_o a) + N_1^2(k_o a)\right)\right].$$

The total unloaded quality factor (Q_o) expression can now be written as

$$(124)\quad Q_o \cong \pi^3 \epsilon\mu^2\omega^3 d a^4 \left(J_1^2(k_o a) - J_o(k_o a)\, J_2(k_o a)\right)\cdot$$

$$\frac{\left(J_1^2(k_o a) + N_1^2(k_o a)\right)}{2\pi^3 a^3 R_s k_o^2 \left[\left(J_o^2(k_o a)\right)\left(J_1^2(k_o a) + N_1^2(k_o a)\right) + \left(J_1^2(k_o a)\right)\left(J_o^2(k_o a) + N_o^2(k_o a)\right)\right] m\delta}$$

$$+ 4\pi^2 \omega\mu d a^2 J_1^2(k_o a)$$

$$+ 4\pi^3 R_s \beta_o^2 a^4 \left(J_1^2(k_o a) - J_o(k_o a)\, J_2(k_o a)\right)\cdot$$

$$\left(J_1^2(k_o a) + N_1^2(k_o a)\right)$$

To check this equation we let $\delta \rightarrow L$ which means that $J_1(k_o a) \rightarrow 0$ and $m\delta \rightarrow d$. Equation 124 reduces to

$$(125) \quad Q_o = \frac{\epsilon\mu^2\omega^3 da}{2R_s\left[k_o^2 d + 2\beta_o^2 a\right]}$$

which can be written in the form

$$(126) \quad Q_o = \frac{\epsilon\mu^2\omega^3 a^3}{2R_s\left[k_o^2 a^2 + \left(\frac{2a}{d}\right)\left(\frac{p\pi a}{d}\right)^2\right]} .$$

Now since the resonant angular velocity for a TE_{01p} mode is given by

$$(127) \quad \omega_r = \frac{1}{a\sqrt{\mu\epsilon}} \sqrt{(k_o a)^2 + \left(\frac{p\pi a}{d}\right)^2}$$

and since $\eta = \left(\frac{\mu}{\epsilon}\right)^{\frac{1}{2}}$ we get

$$(128) \quad Q_o = \frac{\left[(k_o a)^2 + \left(\frac{p\pi a}{d}\right)^2\right]^{3/2}}{2R_s\left[(k_o a)^2 + \left(\frac{2a}{d}\right)\left(\frac{p\pi a}{d}\right)^2\right]} .$$

This last equation is the same as for an unperturbed cavity which means that our derived approximate expression for Q is correct for the limiting case where spaced ring structure approaches a closed cavity condition.

The calculated points for the theoretical curves obtained using Equation 124 are plotted in Figures 10 and 11 for p=1 and p=2, respectively. The measured data are shown in Figures

12 and 13 along with theoretical curves assuming the radiation loss to be negligible. It can be seen here that good correlation results between the theoretical and measured data points for the p=1 case and also for the p=2 case when radiation loss is neglected. Also included is a measured data point for a cavity where the end plates are extended beyond the outside edge of the cavity. The difference between these two conditions does not appear to be very great and thus the neglecting of end effects is partially validated. The theoretical justification for neglecting the radiated power loss in the case of the measured data rests on the fact that the experimental cavity has non-zero wall thickness whereas the derivation was on the basis that (b-a)=0. In the non-zero wall thickness case, one can approximate the fields outside the guide by considering the slots between washers to constitute a radial transmission line of length b-a and thickness L-δ. The only modes considered are the TE_{on} type for a radial line and thus the propagation constant for all of these is imaginary as long as $L-\delta < \lambda/2$. Therefore we have m radial lines excited by the fields inside the guide and operating below cutoff. The mode undergoing the least attenuation in the +r direction is the TE_{01} where the eigenvalue for this case is given by

$$(129) \quad k_r^2 = k^2 - \left(\frac{\pi}{L-\delta}\right)^2$$

Now since the electric fields inside the radial guides must

match the fields at r=a and r=b inside and outside guide, respectively, magnitudes at r=a and r=b must be related to each other by the attenuation of the radial guide. Thus

$$(130)\quad \frac{E^{o}(r=b)}{E^{i}(r=a)} = \frac{K_1(k_r b)}{K_1(k_r a)} = \epsilon^{-jk_r(b-a)}$$

and if one uses the value of $b-a = .9 \times 10^{-2}$ meters and lets $L-\delta \rightarrow L$ then the ratio of field magnitudes inside and outside at f = 10 KMC is given by $\epsilon^{-4.08}$ which means that the radiated power is down by at least 50 times. This suggests that the radiation may be neglected in cases where $L-\delta \ll \lambda/2$ and b-a is sufficiently large. The measurement methods are discussed in the next section and the test data are given in Appendix A. Appendix B gives some fundamental relationships for the unperturbed cavities and the computed values of Q_o and f_r for the various cavities. Because the cavity rings would have to be made extremely thin in the r direction before the experimental data would start to approach the theoretical curves given in Figures 10 and 11, no attempt was made to take experimental data to support these curves.

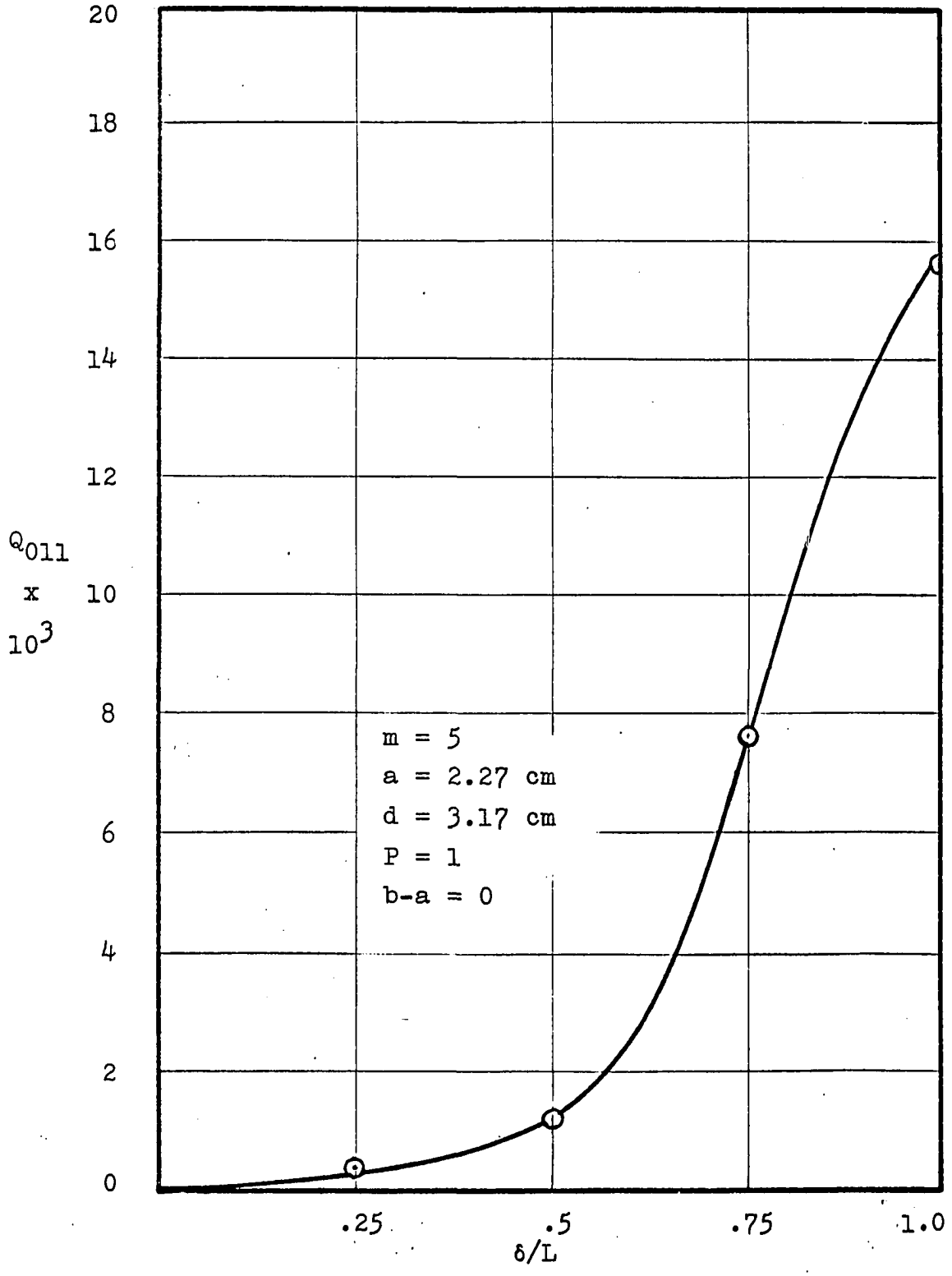

Fig. 10. Theoretical values of cavity Q_{011} versus δ/L

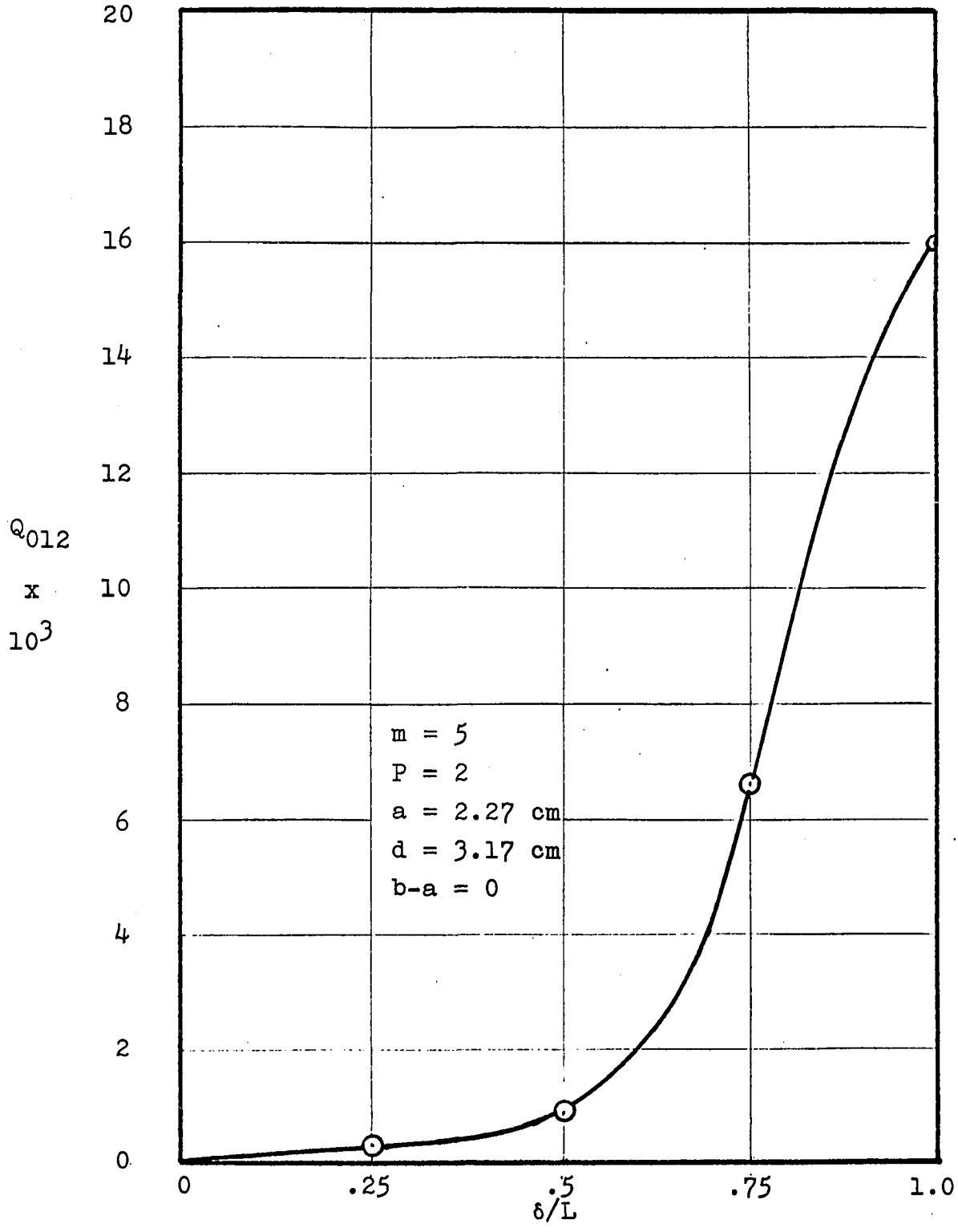

Fig. 11. Theoretical values of cavity Q_{012} versus δ/L

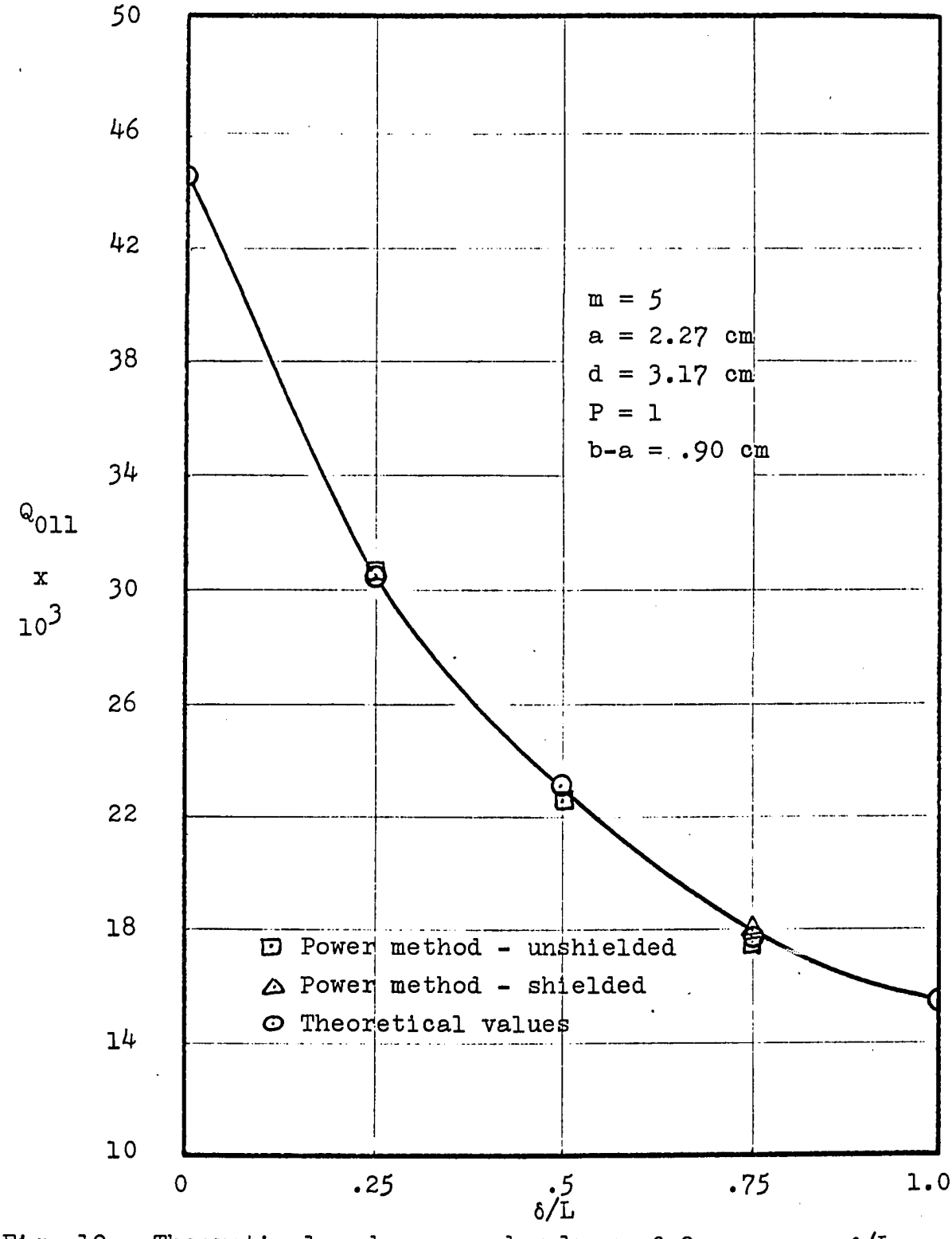

Fig. 12. Theoretical and measured values of Q_{011} versus δ/L

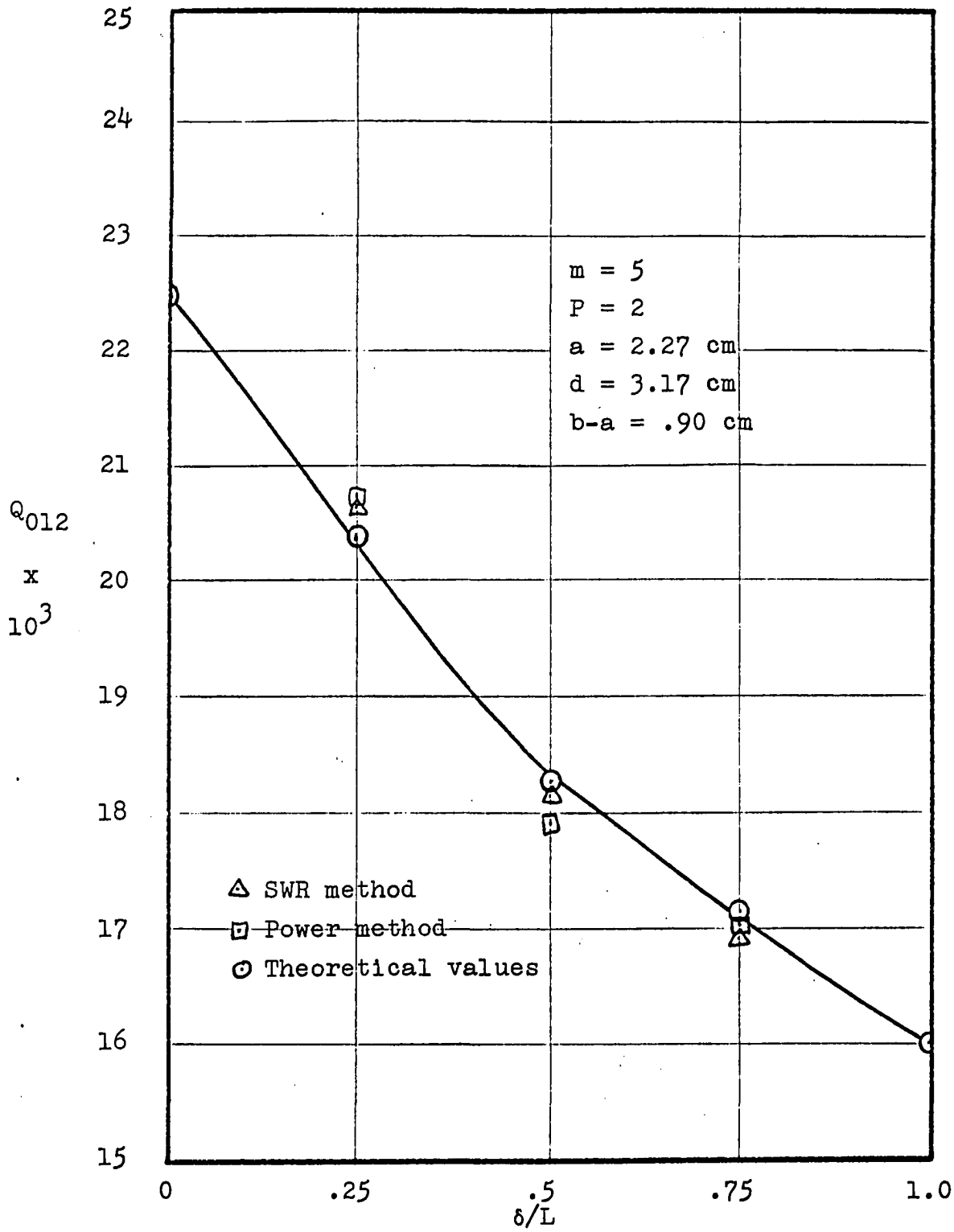

Fig. 13. Theoretical and measured values of Q_{012} versus δ/L

MEASUREMENT TECHNIQUES

Basically there are two general circuit configurations used in a cavity type, microwave refractometer or spectrometer. These two different methods are shown in block diagram form in Figure 14. Although the external microwave circuits differ considerably in the two cases, there is little essential difference in the operation of the cavity.

Reflection Method

First let us consider the reflection type of circuit shown in Figure 14a coupled to the waveguide by a single hole or iris.

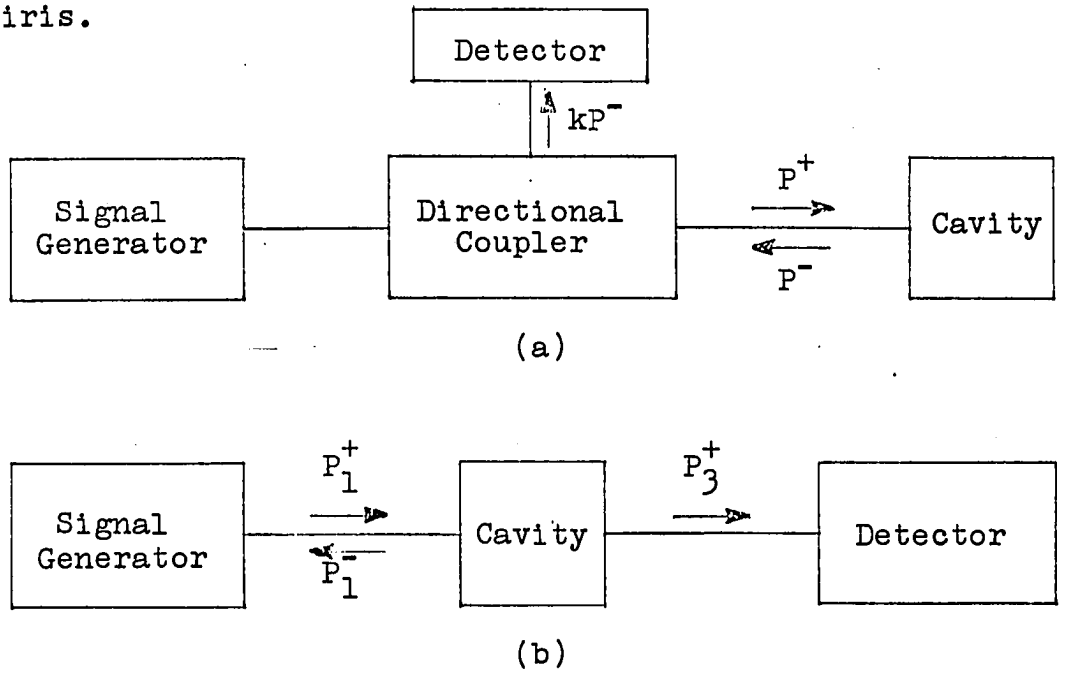

Fig. 14. Resonant cavity measurement circuits

(a) Reflection method

(b) Transmission method

An appropriate equivalent circuit for the cavity and its coupling iris for the reflection method with reference to the bb' plane is shown in Figure 15.

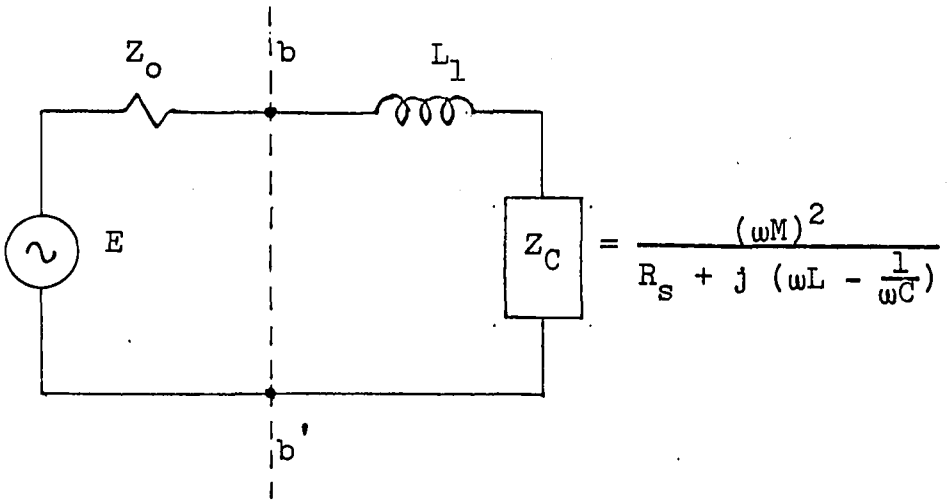

Fig. 15. Equivalent circuit of reflection cavity at plane bb'

In this case the losses in the coupling iris are neglected and M is the mutual inductance between the line and cavity and the cavity is represented by a series R_s,L,C circuit. At plane bb' the impedance looking into the cavity is given by

$$(131) \qquad Z_{bb'} = j\omega L_1 + \frac{(\omega M)^2}{R_s + j\left(\omega L - \frac{1}{\omega C}\right)}$$

thus if we define $\beta_1 = \frac{(\omega M)^2}{R_s Z_o}$ we can write

$$(132) \qquad \frac{Z_{bb'}}{Z_o} = j\,\frac{X_1}{Z_o} + \frac{\beta_1}{1 + j\,\frac{\omega L}{R_s}\left(1 - \left(\frac{\omega_r}{\omega}\right)^2\right)}$$

where $\omega_r^2 = \frac{1}{LC}$. For high Q_o cases $\omega \cong \omega_r$

so that Equation 132 can be written in the form

$$(133) \qquad \frac{Z_{bb'}}{Z_o} = j\frac{X_1}{Z_o} + \frac{\beta_1}{1 + j\,2Q_o\delta}$$

where $\delta = \frac{\omega-\omega_r}{\omega_r}$ and $Q_o = \frac{\omega L}{R_s}$.

The cavity quality factor from Figure 15 can be written as

$$(134) \qquad Q_1 = \frac{\omega L - \beta R_s\, X_1/Z_o}{R_s(1+\beta)}$$

where $\beta = \beta_1 \left(\frac{1}{1 + (X_1/Z_o)^2}\right)$.

Now since in most cases $(X_1/Z_o) << 1$ then $\beta \cong \beta_1$ and we can write

$$(135) \qquad Q_1 \cong \frac{Q_o}{1+\beta} = \frac{Q_o}{1+\beta_1}.$$

Thus we can write that

$$(136) \qquad \frac{1}{Q_1} = \frac{1}{Q_o} + \frac{1}{Q_{x_1}} \qquad \text{where} \qquad \beta_1 = \frac{Q_o}{Q_{x_1}}.$$

Now referring $Z_{bb'}$ to a position aa' nearer the source where the reactance $\frac{X_1}{Z_o}$ is removed then the impedance at the new location is given by

$$(137) \qquad Z_{aa'} = \frac{\beta_1 Z_o}{1 + j\,2Q_o(\delta-\delta_o)}$$

where $\delta_o = \frac{\beta_1}{2Q_o}\left(\frac{X_1}{Z_o}\right)$

and $\delta = \frac{\omega-\omega_r}{\omega_r}$.

But since in general $\frac{X_1}{Z_o} << 1$ and $Q_o >> \beta_1$

then we can write

$$(138) \quad \frac{Z_{aa'}}{Z_o} \simeq \frac{\beta_1}{1 + j\, 2Q_o\delta}.$$

Using Equation 138, one can show that the reflection coefficient near resonance is given by

$$(139) \quad \Gamma_o \simeq \frac{\frac{Z_{aa'}}{Z_o} - 1}{\frac{Z_{aa'}}{Z_o} + 1} = \frac{2\beta_1}{\beta_1 + 1 + j\, 2Q_o\delta}$$

Now if we define $Q_{x_1} = \frac{1}{d_1}$ and $Q_o = \frac{1}{d_o}$ where d_1 and d_o are called loss factors, then $\beta_1 = d_1/d_o$ and Equation 139 can be written in the form

$$(140) \quad \Gamma_o = \frac{2(d_1/d_o)}{\frac{d_1}{d_o} + 1 + j\,\frac{2}{d_o}\,\delta}$$

or

$$(141) \quad \Gamma_o = \frac{2d_1}{d_1 + d_o + j\,2\delta}$$

Assuming now that a lossy material is introduced into the cavity then the new value for d_o is given by $d_o + \frac{\epsilon''}{\epsilon'}$ where the new permittivity is given by $\epsilon' - j\epsilon''$. Thus the reflection coefficient equation can now be written as

$$(142) \quad \Gamma_o' = \frac{2d_1}{d_1 + d_o + \frac{\epsilon''}{\epsilon'} + j\,2Q_o\delta'} = \frac{2d_1}{d_1 + d_o + \epsilon_r'' + j\,2Q_o\delta'}$$

where $\delta' = \frac{\omega - \omega_r'}{\omega_r'}$, $\epsilon_r' = 1$,

and $\omega_r' = \left(\frac{\epsilon''}{\epsilon}\right)\frac{1}{2}\omega_o$.

At resonance with and without a lossy medium, the reflection factors are real and are given by

$$(143) \quad \Gamma'_{o_{res}} = \frac{2d_1}{d_1 + d_o}$$

and

$$(144) \quad \Gamma_{o_{res}} = \frac{2d_1}{d_1 + d_o + \epsilon_r''}$$, respectively.

For $\epsilon_r'' \ll d_1 + d_o$ we can now compute the change in reflected voltage from Equation 145.

$$(145) \qquad \left|\frac{\Delta V^-}{V^+}\right|_{res} = (\Gamma_o - \Gamma_o')_{res} = \frac{2d_1\ \epsilon_r''}{(d_1 + d_o)^2}$$

The maximum change in reflected voltage ΔV^-_{max} for a variable d_1 is given when $d_1 = d_o$ so that

$$(146) \qquad \left|\frac{\Delta V^-_{max}}{V^+}\right| = 2Q_o\ \epsilon_r''$$

or

$$(147) \qquad \Delta V^-_{max} = (2Q_o\ |V^+|)\ \epsilon_r''.$$

The minimum detectable absorption is given by setting ΔV^-_{max} equal to the thermal noise (voltage) given by

$$(148) \qquad V_N(\text{rms}) = (4kTN\Delta f Z_o)^{\frac{1}{2}}.$$

Transmission Method

In the transmission method we are interested in the ratio $\left|\frac{\Delta V_3}{V_3}\right|_{res}$ when a lossy medium of dielectric constant $\epsilon'-j\epsilon''$ is introduced into the sampling cavity. In this case we will develop an expression for the ratio of the power transmitted through the cavity at frequencies near the resonant frequency to the transmitted power at resonance. From this expression we can develop an equation for $\left|\frac{\Delta V_3}{V_3}\right|_{res}$. For this case we consider the coupling holes to be representable by ideal transformers and thus neglect both the losses and the reactance of

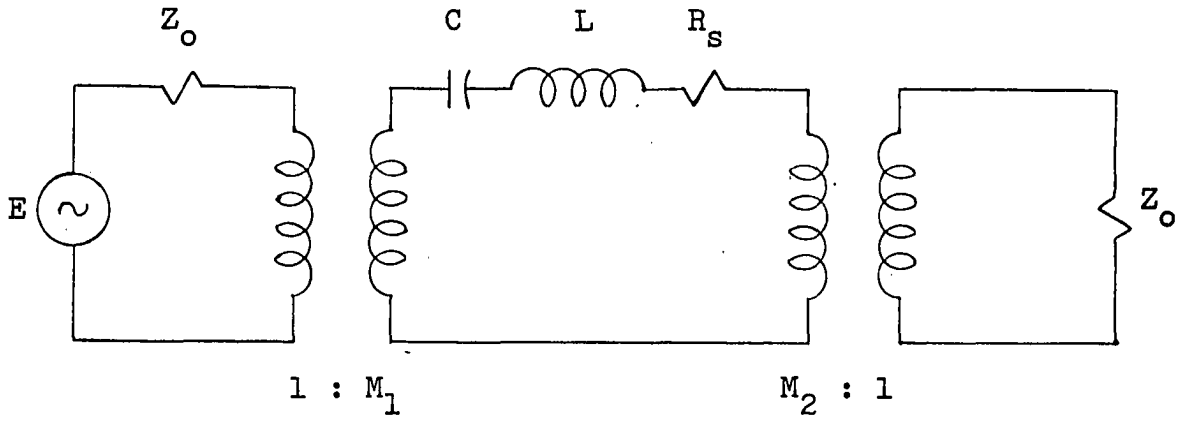

Fig. 16. Equivalent circuit of a transmission cavity

the coupling network. An equivalent circuit for this case is shown in Figure 16. The power transmitted to the load in Figure 16 is given by

$$(149) \qquad P_3 = \frac{1}{2}\left[\frac{n_1^2 \,|E|^2 \, Z_o}{\left|R_s(1+\beta_1+\beta_2) + j(\omega L - \frac{1}{\omega C})\right|^2}\right]$$

and the power transmitted at resonance is then given by

$$(150) \qquad P_{3\ res} = \frac{1}{2}\left[\frac{n_1^2 \,|E|^2 \, Z_o}{R_s^2\,(1+\beta_1+\beta_2)^2}\right]$$

where $\beta_1 = \dfrac{n_1^2 \, Z_o}{R_s}$ and $\beta_2 = \dfrac{n_2^2 \, Z_o}{R_s}$.

The ratio of the power transmitted at frequencies near resonance to the transmitted power at resonance can now be expressed by

$$(151) \qquad \frac{P_3}{P_{3\ res}} \cong \frac{1}{1+4Q_1^2\delta^2}.$$

Since for this case

$$(152) \qquad Q_1 = \frac{1}{d_1+d_2+d_o}$$

where $Q_{X_2} = \frac{1}{d_2}$ and $d_3 = d_1+d_2+d_o$

the corresponding voltage ratio is given by

$$(153) \qquad \left|\frac{V_3}{V_{3\ res}}\right| = \left[\frac{d_3^2}{d_3^2+4\delta^2}\right]^{\frac{1}{2}}$$

Now if we introduce a lossy medium Equation 153 can be written in the form

$$(154) \qquad \left|\frac{V_3'}{V_{3\ res}}\right| = \frac{d_3+\epsilon_r''}{(d_3^2+4\delta'^2)^{\frac{1}{2}}}$$

and since $\delta' = \delta$ in most cases, Equation 154 can be expressed as

$$(155) \qquad \left|\frac{V_3'}{V_{3\ res}}\right| = \frac{d_3+\epsilon_r''}{(d_3^2+4\delta^2)^{\frac{1}{2}}}$$

at frequencies close to resonance.

At resonance where $\delta = 0$ we can now write

$$(156) \qquad \left|\frac{\Delta V_3}{V_{3\,res}}\right| \cong \frac{\epsilon_r''}{d_3} = \frac{\epsilon_r''}{d_o + d_1 + d_2}$$

or

$$(157) \qquad |\Delta V_3| \cong \frac{K_o d_1 \epsilon_r''}{d_3^2}$$

The maximum change in the transmitted voltage at resonance for variables d_1 and d_2 is when $d_1 = d_o + d_2$. This gives the maximum change in ΔV_3 as

$$(158) \qquad \Delta V_{3\,max} = K_o Q_{X_1} \epsilon_r'' = \frac{K_o \epsilon_r''}{d_1}$$

The minimum detectable change in the presence of thermal noise can be computed in the same manner as before.

EXPERIMENTAL METHODS

The two quantities of interest in this paper are the resonant frequency and unloaded quality factor of the cavity being considered. In what follows we will discuss first the measurement of frequency and then the measurement of quality factor for the cavity structures shown in Figures 17, 18, and 19. A typical experimental laboratory set up is shown in Figure 20.

Measurement of Resonant Frequency

There are several methods that can be used in the determination of frequencies in the microwave region. Two of the most important methods are considered here. One of these methods is to measure essentially the wavelength using an absorption type cavity wavemeter which is calibrated in terms of frequency and uses a micrometer dial to measure end plate motion. The most common type of cavity used in a cavity wavemeter is a cylindrical type operating in the TE_{011} mode with an adjustable end plate. The accuracy of this type of measurement is dependent upon temperature, humidity and scale calibration. In most cases the accuracy is within $\pm$ .1%.

The other method used in this research project is shown in Figure 21. It consists basically of a harmonic generator or transfer oscillator and a standard oscillator plus electronic counter. The transfer oscillator frequency is adjusted until a zero beat of nf_1 and f_x is obtained (i.e. $f_2=0$). Then

the standard oscillator frequency is adjusted until it is within 10 MC of f_1. The unknown frequency f_x can then be calculated using the equation

(159) $f_x = n(f_o \pm f_c)$.

If f_o is greater than f_1, the minus sign is used, but if f_1 is greater than f_o the plus sign is used. In order to determine the number of the harmonic n one can adjust the transfer oscillator to the next lower zero beat frequency so that $(n+1)f_1 = f_1'$. Now n can be computed using the expression

(160) $$n = \frac{f_1'/f_1}{1 - f_1'/f_1}$$

Another way to determine the harmonic number n is to measure f_x with a cavity wavemeter and then determine n from

(161) $n = f_x/f_1$.

The accuracy of this method for measuring frequency in the microwave region is about an order of magnitude better than the measurement using a cavity wavemeter.

Measurement of Quality Factor

The various methods that may be used to determine the unloaded quality factor of a cavity are listed below:

(a) Transmission method

(b) Transient or decrement method

(c) Impedance method

(d) Dynamic methods

If we consider a transmission cavity arrangement as shown in Figure 1b the value of Q measured using methods a, b, and d is the loaded Q namely Q_l of Equation 152. For method (a) the value of Q_l is determined by measuring the resonant frequency and the frequencies at the half power transmission points and then using

(162) $Q_l = f_r/\Delta f$.

In the decrement method a pulse of RF at the resonant frequency is applied to the cavity and the decay time of the oscillation after the pulse is removed is measured. The value of Q_l can then be computed by solving the equation

(163) $Q_l = \pi f_r \Delta t$

where Δt = time for oscillation to decay to $1/\epsilon$ of its original value. This method is usually used for cavities with Q_l's higher than 10^4 since Δt is hard to measure accurately below this value of Q. For this reason this method was not employed in the cavity measurements presented in Appendix A. Method (d) uses a swept frequency Klystron source which is caused to sweep in frequency through the resonance curve of the cavity. At the same time this sweep frequency is mixed down to a much lower frequency range by mixing it with a fixed frequency Klystron

source. An adjustable Q circuit at the lower frequency range is adjusted until the response curve for the two swept cavities match. If the transmission detectors are matched then Q_1' can be computed using the equation

$$(164) \quad Q_1 = Q_1'(f_r/f_r')$$

where the primed quantities refer to the low frequency circuit quantities. Since the low frequency loaded quality factor Q_1' can be determined much more accurately than the quality factor Q_1 at the high frequency, it is possible to find Q_1 very accurately using Equation 164. In order to compute Q_o from any of the Q_1 values determined by the methods just mentioned one must be able to measure β_1 and β_2. There are two ways that can be used to determine β_1 and β_2 with sufficient accuracy. One method is to measure P_1^+, P_1^-, and P_3^+ at resonance using the circuit shown in Figure 14b and then compute β_1 and β_2 using the following equations

$$(165) \quad P_2^+/P_1^+ = \frac{4\gamma_1}{(1+\gamma_1)^2} = 1 - \frac{P_1^-}{P_1^+}$$

$$(166) \quad P_3^+/P_2^+ = \frac{\beta_2}{1+\beta_2}$$

and

$$(167) \quad \beta_1 = (1+\beta_2)\,\gamma_1.$$

Another way is to measure the SWR at resonance and note that

$SWR_{(res)} = \gamma_1$ if $\gamma_1 > 1$, otherwise $SWR = \frac{1}{\gamma_1}$. Now if $\beta_2 << 1$ as it is in this case then we can determine β_1 approximately by equating it to γ_1. This method does not of course yield β_2 and for this reason the SWR method is used normally with a reflection type cavity. For the measurements at p = 2 (lower Q_1) the frequency stability of the source was sufficient so that good agreement in the determination of γ_1 was obtained by either method. However, at p = 1 (higher Q_1) this was not so and the power method had to be used.

The measurement of microwave power was accurate to $\pm$ 5%. In order to compute β_1 with sufficient accuracy the same power meter was used to measure both P_1^+ and P_1^- at resonance using directional couplers. One can then assume that any measurement errors will be in the same direction so that an overall accuracy in β_1 should be at least $\pm$ 2%. Since one can measure Q_1 to at least $\pm$ 1%, it seems reasonable to assume that the maximum error in Q_o is approximately $\pm$ 3%.

Impedance methods are perhaps the most accurate of all, but they require a sufficiently stable source so that SWR or phase measurements can be obtained at three or more different frequencies in the resonance curve. It turns out that the most advantageous quantity to measure in order to obtain an accurate Q_1 determination for these high Q_1 cavities is extremely sensitive to changes in source frequency. For this reason the measurements needed could not be made with sufficient accuracy or repeatability. The method of measurement used is noted in Appendix A along with the experimental data.

Fig. 17. Experimental spaced-ring cavity with $\delta/L = 3/4$

Fig. 18. Experimental spaced-ring cavity with $\delta/L = 1/2$

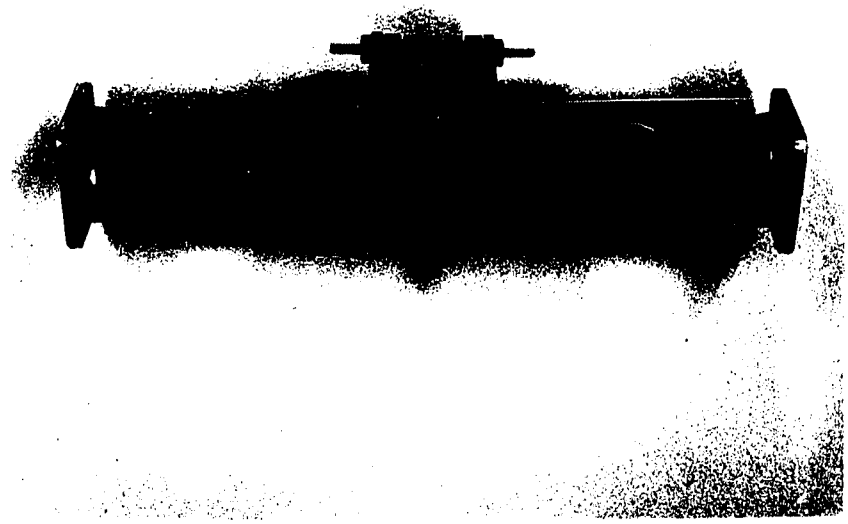

Fig. 19. Experimental spaced-ring cavity with $\delta/L = 1/4$

Fig. 20. Typical experimental laboratory arrangement

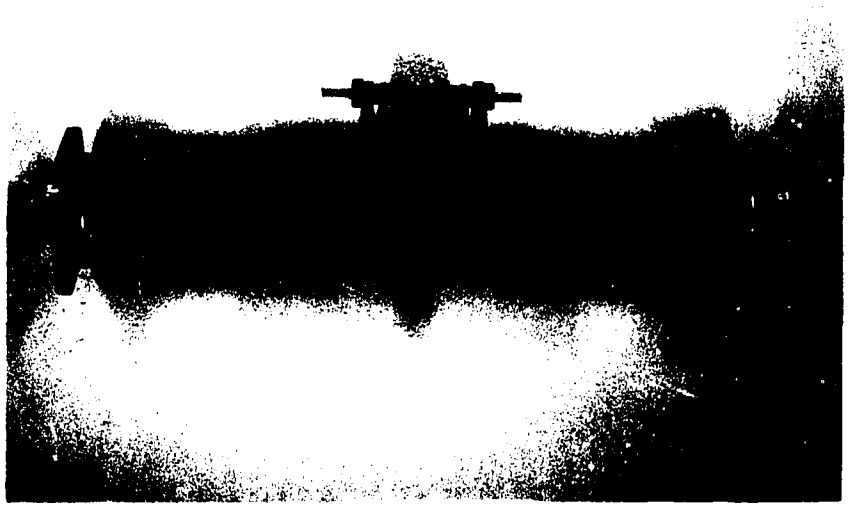

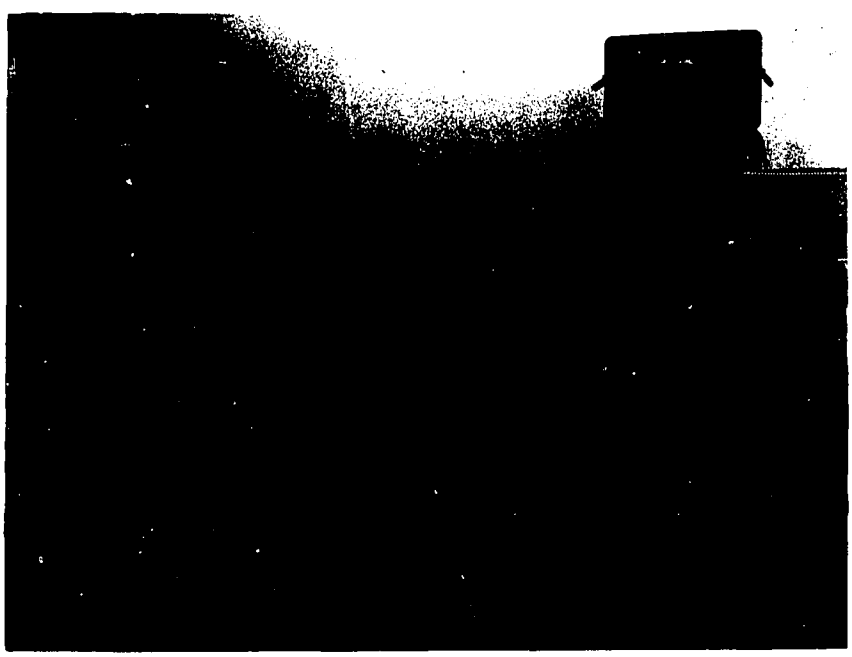

SUMMARY AND CONCLUSIONS

A spaced-ring type of microwave cavity has been considered for use as a sampling cavity in systems used to measure the properties of gaseous media. Those properties of interest were refractive index from which P_{H_2O} can be determined and the absorption spectra from which one can determine the concentration of various polar gas constituents. Also discussed were the important measuring instruments using sampling cavities and the theory upon which their operation is based. From this background, it was shown that the desirable characteristics of a cavity used for these purposes include high quality factor for good sensitivity, stable resonant frequency versus temperature, low turbulence in flow through measurements, and minimum susceptability to absorped gas and adsorbed water vapor on the cavity walls. The characteristics of a spaced-ring type cavity for the case where $\delta/L \rightarrow 0$ yields a structure which is improved over present cavities in all of the above factors.

In the analysis of this type of cavity, it has been shown that the technique of space-harmonics is quite valid for the range of δ/L considered and could be extended to lower ratios if m were increased. The ratio of open to closed cavity area to one dimensional transverse flow of gas is given by

$$A_{open}/A_{closed} = \frac{1 - \delta/L}{\delta/L}.$$

By decreasing the ratio of δ/L the turbulence caused by the rings in the flowing gas could be made quite small. This would tend to increase the frequency response and accuracy of the instrument using the cavity by decreasing the amount of mixing and the net wash-out time.

The approximation $J_1(k_o a) << N_1(k_o a)$ used in the solution of the determinal equation was shown to be valid in the cases considered for the TE_{011} mode and the TE_{012} mode. For lower δ/L values $J_1(k_o a)$ will become larger. This may cause the approximation made in order to solve the determinal equation to become somewhat less valid. This effect can be counteracted, however, by increasing m without lowering A open/A closed. The extension of this technique to larger L values or smaller values of m is quite possible. In general, however, as L is increased for a given b-a dimension the radiation term will continue to increase and may not be negligible. The value of Q_o will be decreased if the radiation loss becomes significant compared to the wall losses. Also, this same type of effect would be present if b-a were reduced with other dimensions held constant.

Although several terms were neglected in the final Q_o equation, it turns out that each is quite small for the cases considered here compared to the terms retained. This is also born out by the close comparison of the theoretical values and the experimental data. As the magnitude of the space harmonics

outside the cavity approach those inside the cavity, the assumption neglecting end effects outside the cavity may not be valid. This factor could be removed by extending the end plates in the +r direction for some reasonable length beyond r = b.

It has been shown conclusively that this type of cavity is well suited for the applications considered and that it can be adequately described by the method of space harmonics for wide ranges in physical configuration. Therefore, it seems reasonable to suggest that further work directed toward the design of a cavity of this type for an application where it can be advantageously employed should be undertaken.

LITERATURE CITED

1. Bean, B. R. The radio refractive index of air. Institute of Electrical and Electronic Engineers Proceedings 50: 260-273. 1962.

2. Birnbaum, G. A recording microwave refractometer. Rev. Sci. Instr. 21: 169-176. 1950.

3. Birnbaum, G. and Chatterjee, S. K. The dielectric constant of water vapor in the microwave region. J. Appl. Phys. 23: 220-223. 1952.

4. Birnbaum, G. Kryder, S. J., and Lyons, H. Microwave measurements of the dielectric properties of gases. J. Appl. Phys. 22: 95-102. 1951.

5. Brown, G. R., Sharpe, R. A., and Hughes, W. L. Lines, waves, and antennas. New York, N.Y., The Ronald Press Co., Inc. 1961.

6. Ginzton, Edward L. Microwave measurements. New York, N.Y., McGraw-Hill Book Co., Inc. 1957.

7. Harrington, Roger F. Time-harmonic electromagnetic fields. 1st ed. New York, N.Y., McGraw-Hill Book Co., Inc. 1961.

8. Lebowitz, R. A. Determination of the parameters of cavities terminating transmission lines. Institute of Radio Engineers Trans. on Microwave Theory 4: 51-53. 1956.

9. Lerner, D. S. and Wheeler, H. A. Measurement of bandwidth of microwave resonator by phase shift of signal modulation. Institute of Radio Engineers Trans. on Microwave Theory and Techniques MTT-8: 343-345. 1960.

10. Magee, J. B. and Crain, C. M. Recording microwave hygrometer. Rev. Sci. Instr. 29: 51-54. 1958.

11. Matthaei, G. L. and Weller, D. B. Circular TE_{011}-mode, trapped-mode band-pass filters. Institute of Electrical and Electronic Engineers Transactions on Microwave Theory and Techniques MTT-13: 581-589. 1965.

12. McLachlan, N. W. Bessel functions for engineers. 2nd ed. London, England, Oxford University Press. 1948.

13. Miller, S. E. Waveguide as a communication medium. The Bell System Technical J. 33: 1209-1265. 1954.

14. Miller, S. E. and Beck, A. C. Low-loss waveguide transmission. Institute of Radio Engineers Proceedings 41: 348-358. 1952.

15. Miller, S. E. and Beck, A. C. Notes on method of transmitting the circular electric waves around bends. Institute of Radio Engineers Proceedings 40: 1104-1113. 1952.

16. Moreno, Theodore. Microwave transmission design data. 1st ed. New York, N.Y., Dover Publications, Inc. 1958.

17. Mullen, Paul W. Modern gas analysis. 1st ed. New York, N.Y., Interscience Publishers, Inc. 1955.

18. Pierce, J. R. Coupling of modes of propagation. J. Appl. Phys. 25: 179-183. 1954.

19. Ramo, Simon and Whinnery, J. R. Fields and waves in modern radio. 2nd ed. New York, N.Y., John Wiley and Sons, Inc. 1953.

20. Sensiper, S. Electromagnetic wave propagation on helical conductors. Microfilm copy. Unpublished Sc.D. thesis. Cambridge, Mass., Library, Massachusetts Institute of Technology. 1951.

21. Slater, J. C. Microwave electronics. Princeton, New Jersey, D. Van Nostrand Company, Inc. 1950.

22. Smith, E. K. and Weintraub, S. The constants in the equation for atmospheric refractive index at radio frequencies. Institute of Radio Engineers Proceedings 41: 1035-1037. 1953.

23. Townes, C. H. and Schawlow, A. L. Microwave spectroscopy. New York, N.Y., McGraw-Hill Book Co., Inc. 1955.

24. Vetter, M. M. and Thompson, M. C., Jr. An absolute microwave refractometer. Rev. Sci. Instr. 33: 656-660. 1962.

25. Watkins, Dean E. Topics in electromagnetic theory. New York, N.Y., John Wiley and Sons, Inc. 1958.

26. Widder, David V. Advanced calculus. 1st ed. New York, N.Y., Prentice-Hall, Inc. 1947.

ACKNOWLEDGEMENTS

The author wishes to express his appreciation to his major professor Dr. D. W. Gade for his help during the preparation of this manuscript and to Dr. R. E. Post for his suggestion of the topic and helpful comments.

Also, the writer would like to extend his thanks to all the members of the Department of Electrical Engineering who expressed an interest in this research, to Mr. J. T. McConnell for his help in the construction of the experimental units, and to his wife for her understanding and encouragement.

APPENDIX A

The experimental data given in Table 1 was obtained in the laboratory using the circuits shown in Figures 22 and 23. The values for β_2 for the standing wave ratio measurement are estimated values based on those obtained in the power measurement method for the same cavity. As previously mentioned the SWR method could not be used at the lower frequency because the value of Q_1 was too large and the frequency stability of the source was not good enough to allow accurate and repeatable measurements of SWR at cavity resonance.

Table 1. Experimental data for spaced-ring cavities

p	δ/L	γ_1	β_1	β_2	Δf	f_o	Q_1	Q_o
1	1/4	7.68	7.77	.0125	2.67	9.12	3240	30,500
1	1/2	6.30	6.36	.0100	3.00	9.198	3070	22,600
1[a]	3/4	7.75	7.78	.0070	4.03	9.304	2310	18,000
1	3/4	7.55	7.59	.0065	4.49	9.306	2080	17,900
2	1/4	16.4	17.5	.070	1.43	12.12	1120	20,800
2	1/2	16.0	17.0	.060	1.23	12.16	990	17,900
2	3/4	20.7	21.6	.043	1.64	12.37	753	17,050
2[b]	3/4	19.8	20.6	.040	1.58	12.36	780	16,900
2[b]	1/2	22.6	23.7	.050	1.65	12.17	735	18,200
2[b]	1/4	24.2	25.6	.060	1.56	12.13	780	20,700

[a]Data for cavity with extended end plates.

[b]Data from SWR measurements.

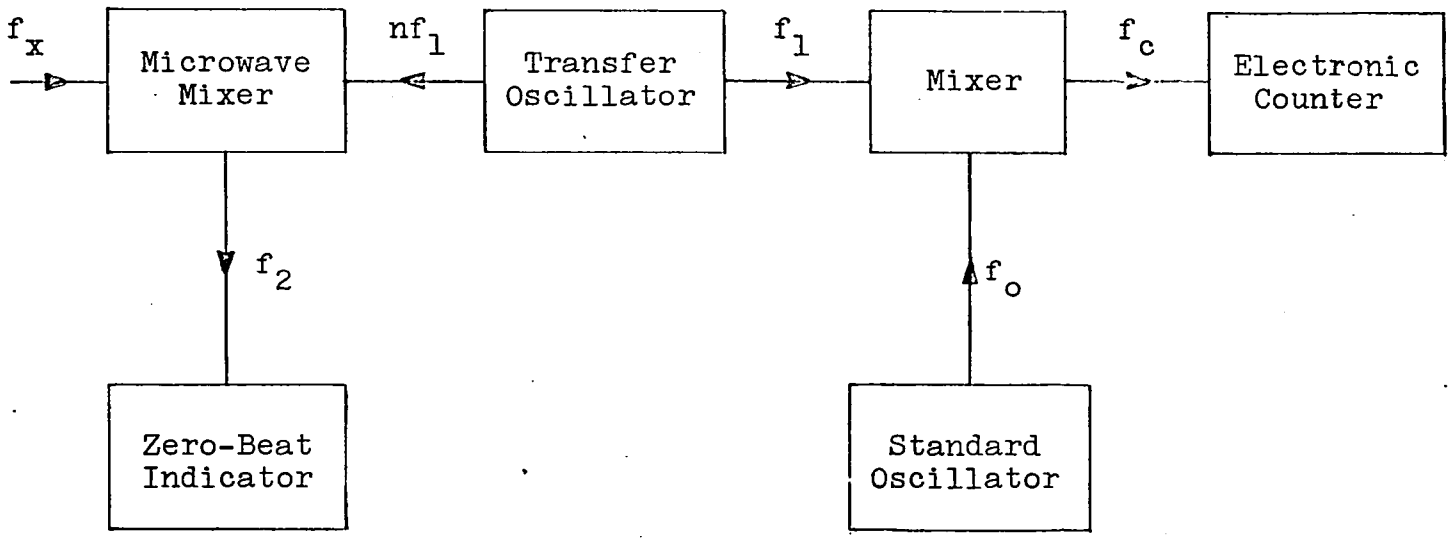

Fig. 21. Block diagram of equipment used in frequency determination

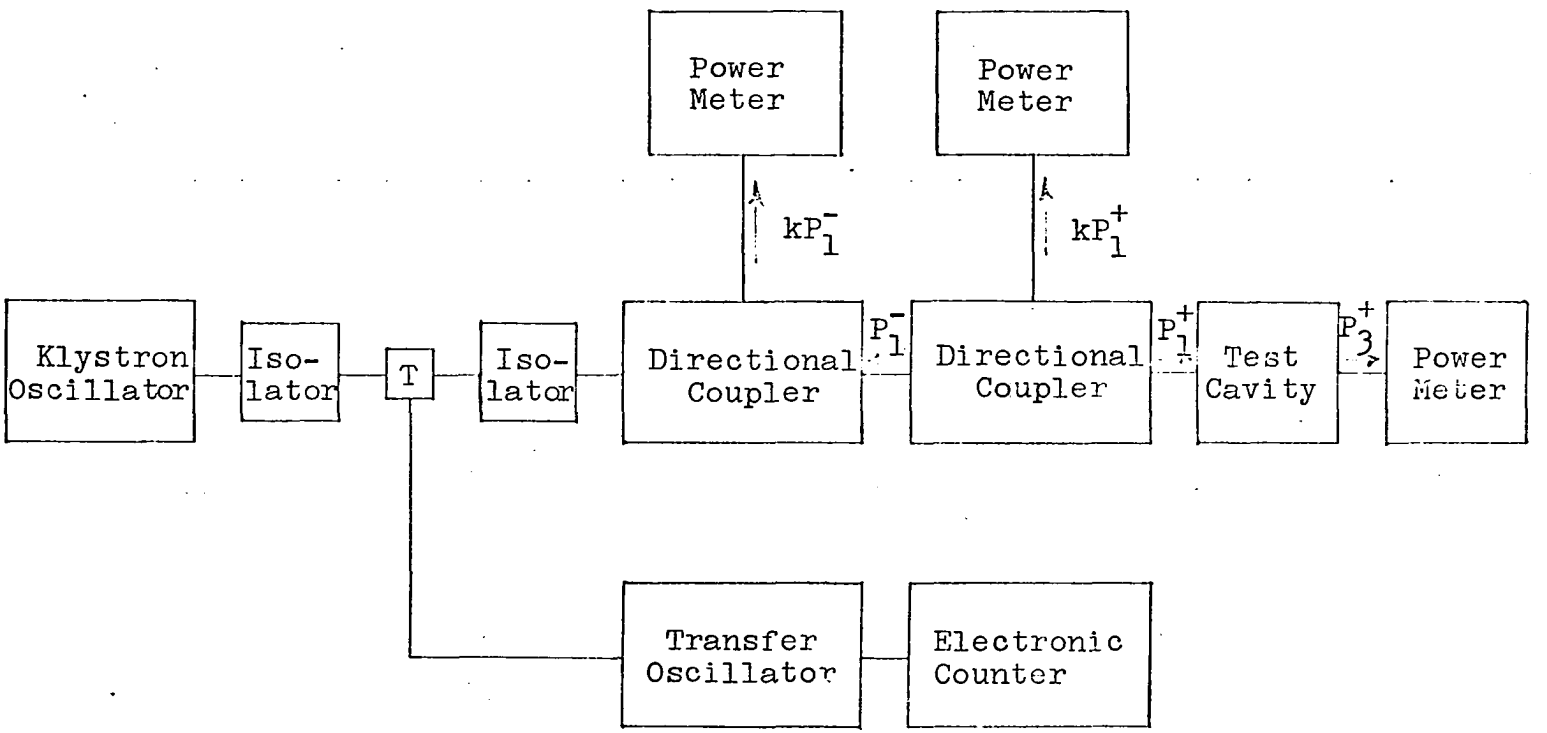

Fig. 22. Block diagram of experimental circuit used for power measurements

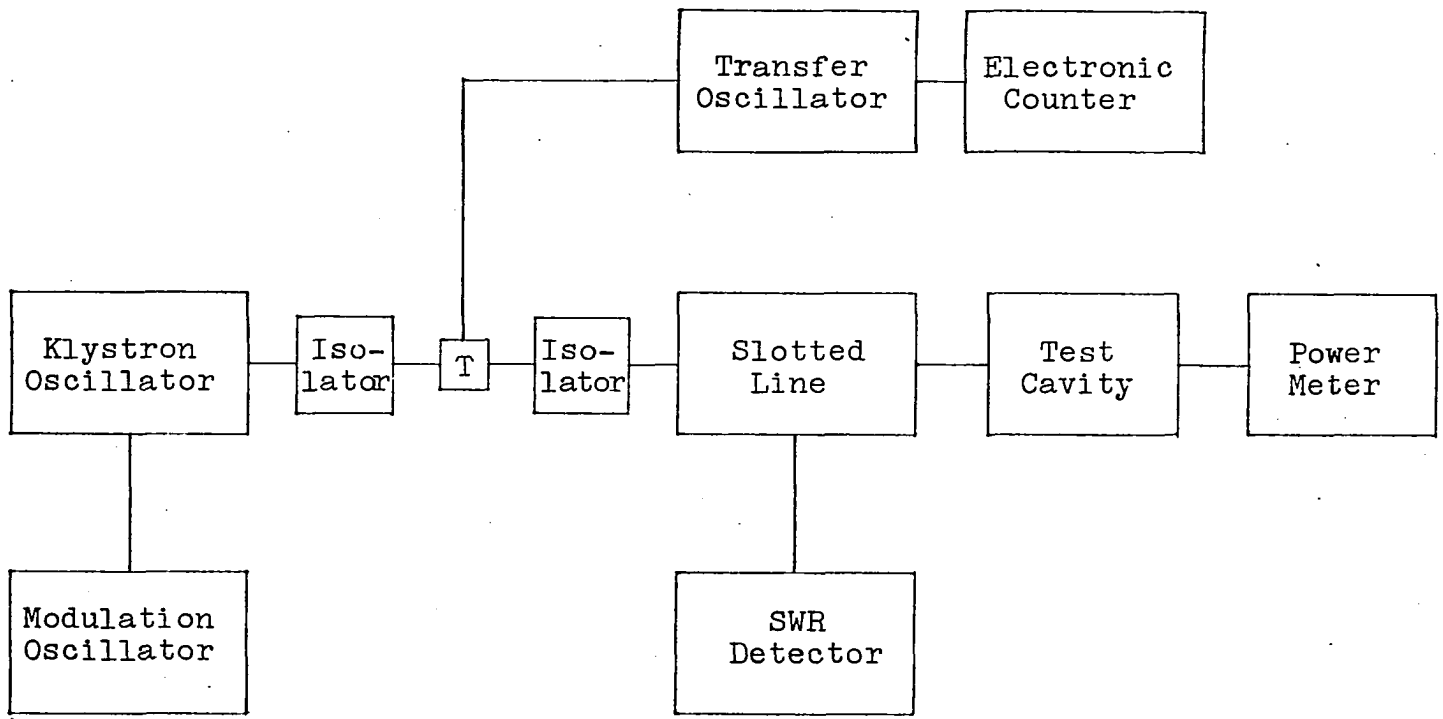

Fig. 23. Block diagram of experimental circuit used for SWR measurements

APPENDIX B

Using the dimensions of $a = 2.27 \times 10^2$ and $d = 3.17 \times 10^2$, we can compute the resonant frequencies and the unload Q values for a cavity without openings (unpertabated). These values are given in the table below for the TE_{011} and TE_{012} modes. The equations of interest are

$$(168) \quad f'_{r_{mnp}} = \frac{1}{2\pi a\sqrt{\mu\epsilon}}\sqrt{\tau'^2_{np} + \left(\frac{p\pi a}{d}\right)^2}$$

and

$$(169) \quad Q'_{r_{mnp}} = \frac{\left[\tau'^2_{mn} + \left(\frac{p\pi a}{d}\right)^2\right]^{3/2}\left(\tau'^2_{mn} - m^2\right)}{2R_s\left[\tau'^4_{mn} + \frac{np\pi a}{d} + \frac{2a}{d}\left(\frac{p\pi a}{d}\right)^2\left(\tau'^2_{mn} - m^2\right)\right]}$$

where $R_s = 5 \times 10^{-7}\sqrt{f}$ for brass and $\eta = 377$. For a cavity made of brass with the dimensions given above the quantities of interest are listed in Table 2.

Table 2. Computed values for unperturbed brass cavity

Mode	f'_r	Q'_o	τ'_{01}
TE_{011}	9.3	15,600	3.83
TE_{012}	12.4	16,000	3.83

In the computations of Q_o and f_r for the various cavity structures the following equations were used.

$$(170)\quad \pi N_1(k_o a)\, J_1(k_o a) \cong \sum_{n\neq o} \frac{1}{\tau_n a} \left[\frac{\sin \frac{\beta_n \delta}{2}}{\frac{\beta_n \delta}{2}}\right]^2$$

$$(171)\quad \tau_n a = \sqrt{4\pi^2 m^2 \left(\frac{a}{d}\right)^2 \left(\frac{np}{m} + n^2\right) - k_o^2 a^2}$$

$$(172)\quad \frac{f_{r_{011}}}{f'_{r_{011}}} = \left\{\frac{(k_o a)^2 + \left(\frac{p\pi a}{d}\right)^2}{(\tau'_{01})^2 + \left(\frac{p\pi a}{d}\right)^2}\right\}^{1/2}$$

$$(173)\quad Q_o \cong \frac{\pi^3 \varepsilon \mu^2 \omega^3 d a^4 \quad (J_1^2(k_o a) - J_o(k_o a)\, J_2(k_o a))}{2\pi^3 a^3 R_s k_o^2 \quad J_o^2(k_o a)\, (J_1^2(k_o a) + N_1^2(k_o a)) +}$$

$$\frac{(J_1^2(k_o a) + N_1^2(k_o a))}{J_1^2(k_o a)\, (J_o^2(k_o a) + N_o^2(k_o a)) \quad m\delta}$$

$$\overline{+ 4\pi^2 \omega \mu d a^2 J_1^2(k_o a)}$$

$$\overline{+ 4\pi^3 R_s \beta_o^2 a^4 (J_1^2(k_o a) - J_o(k_o a)\, J_2(k_o a))} \cdot$$

$$\overline{(J_1^2(k_o a) + N_1^2(k_o a))}$$

Using Equations 170 and 171 in an iterative fashion we obtain a value for $k_o a$. Then we can solve for $f_{r_{011}}/f'_{r_{011}}$ and also for Q_o. The calculated values obtained are given in Table 3.

Table 3. Theoretical data for spaced-ring cavities

Mode	$k_o a$	δ/L	f_r	Q_o^*	Q_o^Δ
TE_{011}	3.69	1/4	9.10	296	30,300
"	3.76	1/2	9.20	1132	22,900
"	3.81	3/4	9.30	7650	17,750
TE_{012}	3.65	1/4	12.10	154	20,500
"	3.75	1/2	12.17	780	18,250
"	3.81	3/4	12.33	6670	17,200

$^*b-a = 0$ radiated power not negligible.

$^\Delta b-a \neq 0$ radiated power neglected.

APPENDIX C

The question naturally arises about the convergence of the summation in Equation 67 for $\delta/L > 0$. In order to show that this infinite sum does indeed become bounded as n $+\infty$ or $-\infty$, we proceed as follows.

First let us break the right hand side of Equation 67 into two parts so that

$$(174) \quad \sum_{n\neq o} K_1(\tau_n a)\, I_1(\tau_n a) \left[\frac{\sin \frac{\beta_n \delta}{L}}{\frac{\beta_n \delta}{L}}\right]^2$$

becomes

$$(175) \quad \sum_{n=-1}^{-\infty} K_1(\tau_n a)\, I_1(\tau_n a) \left[\frac{\sin \frac{\beta_n \delta}{L}}{\frac{\beta_n \delta}{L}}\right]^2$$

$$+ \sum_{n=1}^{\infty} K_1(\tau_n a)\, I_1(\tau_n a) \left[\frac{\sin \frac{\beta_n \delta}{L}}{\frac{\beta_n \delta}{L}}\right]^2$$

where

$$(176) \quad \tau_n a = (An^2 + Bn - C)^{\frac{1}{2}}$$

and

$$(177) \quad \beta_n = \beta o + \frac{2\pi n}{L}.$$

Since for all cases considered A, B, and C are positive real with $A > B > C$ and $A > B + C$, one can show that for all $n \neq 0$ $\tau_n a$ is positive real if we selected the positive root from Equation 176. Also the argument $\tau_n a$ for $n < o$ is always less than the argument $\tau_n a$ for $n > o$. This causes the first summation in Equation 175 to be term by term greater than the second summation. Thus if one can show that

$$(178) \quad \sum_{n=-1}^{-\infty} K_1(\tau_n a)\, I_1(\tau_n a) \left[\frac{\sin \frac{\beta_n \delta}{L}}{\frac{\beta_n \delta}{L}} \right]^2$$

converges then certainly the summation in Equation 174 converges. Rewriting Equation 178 we get

$$(179) \quad \sum_{m=1}^{\infty} K_1(\tau_m a)\, I(\tau_m a) \left[\frac{\sin \frac{\beta_m \delta}{L}}{\frac{\beta_m \delta}{L}} \right]^2$$

where $m = -n$,

$$\tau_m a = (A_m^2 - Bm - C)^{\frac{1}{2}},$$

and $$\beta_m = \beta_o - \frac{2\pi m}{L}.$$

If we define $x = \frac{\beta_m \delta}{L}$ then we can write that

$$(180) \quad \left(\frac{\sin x}{x} \right)^2 < \frac{1}{\left(\frac{2\pi m}{L} - \beta_o \right) \delta / L}$$

since $\beta_o < \frac{2\pi m}{L}$ for all $m > o$ and

(181) $$\left(\frac{\sin x}{x}\right)^2 < \frac{1}{x} \quad .$$

Since $K_1(\tau_m a)\, I_1(\tau_m a) < \frac{1}{2\tau_m a}$ for all $m > o$ we can write that the

(182) $$\sum_{m=1}^{\infty} K_1(\tau_m a)\, I_1(\tau_m a) \left[\frac{\sin \frac{\beta_m \delta}{L}}{\frac{\beta_m \delta}{L}}\right]^2$$

$$< \sum_{m=1}^{\infty} \frac{1}{2\,(Am^2 - Bm - C)^{\frac{1}{2}}\,(\frac{2\pi m}{L} - \beta_o)\,\delta/L}$$

The summation on the right hand side of Equation 182 converges since it behaves like $1/m^2$ for large m. Thus the left hand equation is bounded and so the summation of Equation 174 is also bounded.